

Dynamical diffraction in sinusoidal potentials: uniform approximations for Mathieu functions

D H J O'Dell

Chemical Physics Department, Weizmann Institute of Science,
Rehovot 76100, Israel

June 9, 2024

Abstract

Abstract. Eigenvalues and eigenfunctions of Mathieu's equation are found in the short wavelength limit using a uniform approximation (method of comparison with a 'known' equation having the same classical turning point structure). The applicability of the uniform approximation method relies upon the fact that by passing into Fourier space the Mathieu equation can be mapped onto the simpler problem of a double well potential. The resulting eigenfunctions (Bloch waves), which are uniformly valid for all angles, are then used to describe the semiclassical scattering of waves by potentials varying sinusoidally in one direction. In such situations, for instance in the diffraction of atoms by gratings made of light, it is common to make the Raman-Nath approximation which ignores the motion of the atoms inside the grating. When using the eigenfunctions no such approximation is made so that the dynamical diffraction regime (long interaction time) can be explored.

1. Introduction Consider a diffraction experiment in two dimensions, as depicted in Figure 1. A plane wave $\exp(ikz)$ propagates freely in the \hat{z} (longitudinal) direction and is incident normally upon a medium with a refractive index which varies weakly in the \hat{x} (transverse) direction

$$n(x) = n_0 + n_1 \cos 2Kx \quad (n_1 \ll n_0). \quad (1)$$

As the refractive index depends only on x , the wavefunction inside the medium separates, $\Psi(z, x) = \phi(z)\psi(x)$, with $\phi(z)$ being trivially given by

$$\phi(z) = \exp\left(iz\sqrt{k^2 n_0^2 - \kappa}\right) \quad (2)$$

with κ a separation constant proportional to the transverse energy of the wave inside the medium. The transverse behaviour is governed by Mathieu's equation (see Abramowitz and Stegun [1])

$$\frac{\partial^2 \psi(x)}{\partial x^2} + (\kappa + 2k^2 n_0 n_1 \cos 2Kx) \psi(x) = 0. \quad (3)$$

More generally, Mathieu's equation is obtained whenever the 3-dimensional Helmholtz wave equation is separated in elliptical coordinates, useful for, say, scattering from elliptical boundaries. This paper is concerned with the short wavelength (semiclassical) regime for which the parameter $2k^2 n_0 n_1 / K^2$ is very large. One motivation is that the resulting asymptotics are known to describe the emergence of interesting classical features such as caustics (singularities of the geometric ray theory) which come to dominate the wave field as the wavelength is reduced to zero. The caustic structure becomes ever more intricate as the (longitudinal) thickness of the medium is increased (Berry and O'Dell [8] (1999)).

Diffraction by a sinusoidal grating has been studied in the context of the diffraction of light by ultrasound since at least 1921 (Brillouin [9] (1921)) (see Berry [3] (1966) for a review to 1966). More recent interest has arisen through the realisation of the diffraction of beams of atoms by beams of light (Adams *et al* [2] (1994)). Then $n(x) = \sqrt{1 - V(x)/E}$, where E is the energy of the atoms and $V(x)$ is the potential energy due to their interaction with a standing wave of light (Cohen-Tannoudji *et al* (1992) [10], Kazantsev *et al* (1991) [15])

$$V(x) = -\frac{\Delta}{4\hbar} \frac{d^2 \mathcal{E}_0^2}{\Delta^2 + \Gamma^2/4} \cos^2 Kx = -V_0 \cos^2 Kx \quad (4)$$

with \mathcal{E}_0 the magnitude of the electric field of the counter propagating laser beams which form the standing wave, K their wavenumber and Δ the frequency detuning from resonance. Γ is the spontaneous decay rate for the excited atom and d the atomic dipole moment for the electronic transition being used.

The resonant nature of the atom-light interaction allows for an efficient transfer of transverse kinetic energy to the atoms. Combined with their large mass, this means the atoms can attain small transverse de Broglie wavelengths and so are rather good candidates to access the semiclassical scattering regime when compared with other microscopic particles such as neutrons or electrons.

The idealised experiment described above assumes that the standing wave laser field has a ‘top-hat’ cross-section in the longitudinal direction, switching on at $z = 0$, and remaining constant till switching off at $z = Z$ at which point the atoms propagate undisturbed to a detector in the farfield. One might achieve this by telescopically expanding the normally gaussian laser profile and physically masking the entry and exit edges to make them sharp (diffraction limited). In this way the entry and exit into the laser can be sudden from the point of view of the dynamics of the centre of mass of the atom, but still adiabatic from the point of view of the rapid Rabi oscillations of the internal electronic states that generate the potential given by Equation (4), see O’Dell [16] (1999) for more details. In any case, features such as caustics will still be qualitatively correctly described by the simple model given here even if experimental conditions differ considerably. This is because caustics are stable to perturbations as guaranteed by the optical catastrophe theory (Berry [6] (1980)).

2. Dynamical diffraction and the Raman-Nath equations

The time independent Schrödinger equation governing the passage of atoms of energy $E = \hbar^2 k^2/2m$ through an optical standing wave of periodicity π/K is

$$\frac{\partial^2 \Psi}{\partial x^2} + \frac{\partial^2 \Psi}{\partial z^2} + \left(k^2 + \frac{2mV_0}{\hbar^2} \cos^2(Kx) \right) \Psi = 0. \quad (5)$$

The periodic potential suggests an atomic wavefunction of the form

$$\Psi(x, z) = e^{ikz} \sum_{n=-\infty}^{\infty} A_n(z) e^{2inKx}. \quad (6)$$

An advantage of this decomposition of the wavefunction is that upon exiting the interaction region at $z = Z$, the terms in Equation (6) represent freely propagating diffracted waves travelling at angles $\arcsin(2nK/k)$ to the z axis with amplitudes $A_n(z = Z)$. A detector in the farfield will register a diffraction pattern made up of discrete beams with intensities $|A_n(Z)|^2$. The amplitudes satisfy $\sum_{n=-\infty}^{+\infty} |A_n|^2 = 1$. The rest of this paper is devoted to determining the $A_n(z)$.

If the initial kinetic energy of the atoms is thermal then $k \gg K$ and the propagation of the atom beam is paraxial. The paraxiality means that the evolution of the A_n with z will be much slower than $\exp(ikz)$ so when substituting (6) into (5) terms containing $d^2 A_n/dz^2$ can be ignored. The result is an infinite series of coupled equations

$$i \frac{\partial A_n}{\partial \zeta} - n^2 A_n + \frac{\Lambda}{2} (A_{n+1} + 2A_n + A_{n-1}) = 0 \quad (7)$$

where

$$\zeta \equiv \frac{2K^2 z}{k} \quad , \quad \Lambda \equiv \frac{mV_0}{4\hbar^2 K^2}. \quad (8)$$

The parameter Λ is equivalent to the parameter $2k^2 n_0 n_1 / K^2$ appearing above in Eq. (3)—by letting $\hbar \rightarrow 0$, and hence $\Lambda \rightarrow \infty$, one obtains the classical limit. Of course, taking the limit $\hbar \rightarrow 0$ is a formal device. In an actual experiment the short wavelength limit is approached by, say, making V_0 , the interaction between the atoms and the light, as large as possible. This increases the depth of the wells of the sinusoidal potential which in turn means there are more quantised transverse states. A phase transformation $A_n \rightarrow A_n \exp(i\Lambda\zeta)$ slightly simplifies the equations to

$$i \frac{\partial A_n}{\partial \zeta} - n^2 A_n + \frac{\Lambda}{2} (A_{n+1} + A_{n-1}) = 0. \quad (9)$$

These are (apart from a straight forward change of variables) the differential difference equations introduced by Raman and Nath [18, 19] (1935, 1936) to describe the diffraction of light by ultrasound. The Raman-Nath (RN) equations are a description of dynamical diffraction, yielding the evolution of the amplitudes of the various diffracted beams as the atom wave passes through the light grating. In their original paper, Raman and Nath [18] (1935) observed that by ignoring the diagonal term, $n^2 A_n$, one obtains simple solutions for A_n in terms of Bessel functions. This is equivalent to neglecting the transverse kinetic energy of the atoms and the sinusoidal potential then acts only as a pure phase grating, see Berry [3] (1966). This is a very successful approximation for short interaction times (Sanders (1936), Gould *et al* (1986), Rasel *et al* (1995) [21, 13, 20]) but *dynamical* diffraction requires that full account be taken of the transverse motion.

A general property of paraxial systems is that the axial coordinate, in this case the rescaled longitudinal distance, ζ , plays the rôle of time. The numerical integration of the RN equations is relatively simple since they are first order differential equations in ζ with only a single boundary condition: $A_n(\zeta = 0) = \delta_{n0}$. However, when investigating the behaviour at long interaction times it becomes more economic to analyse the problem in terms of the eigenfunctions of the scattering potential, which propagate unchanged through the medium. This approach will be adopted by seeking eigenfunctions of the RN equations (9) of the form $A_n \equiv B_n \exp(-iE\zeta)$. Corresponding to each eigenvalue E^j is an eigenfunction consisting of a ‘vector’ of amplitudes $(B_{-\infty}^j, \dots, B_{-2}^j, B_{-1}^j, B_0^j, B_1^j, B_2^j, \dots, B_{\infty}^j)$, whose elements satisfy

$$E^j B_n^j = n^2 B_n^j - \frac{\Lambda}{2} (B_{n+1}^j + B_{n-1}^j). \quad (10)$$

This equation defines the tridiagonal RN matrix hamiltonian. For a weak potential (i.e. small Λ : the quantum, non-classical limit) the RN matrix can be approximated by a 3×3 , or for the special case of oblique incidence near a Bragg angle, a 2×2 matrix, and analytical solutions for the Bloch waves (eigenfunctions) are easy to find (Berry and O’Dell [7] (1998)). Here, however, we are interested in the opposite limit.

For the purposes of numerical diagonalisation, a guide to the minimum diffraction order, $\pm N$, at which the RN matrix can be safely truncated for large Λ is given by

$$N = \sqrt{2\Lambda} \propto \hbar^{-1}. \quad (11)$$

This includes only those beams contained within the maximum scattering angle that can be achieved *classically* (Berry (1966)). Criterion (11) becomes exact as $\Lambda \rightarrow \infty$ but at the cost of requiring an infinite number of beams.

The ‘physical’ derivation of the stationary RN equation (10) given here is nothing more than a Fourier analysis of Mathieu’s equation (3). Equation (10) is the recursion relation satisfied by the Fourier coefficients of periodic solutions to Mathieu’s equation: the even and odd *Mathieu functions* (Abramowitz and Stegun [1] (1964)). The eigenvalues E^j are known as the *characteristic values*.

3. WKB solution of the Raman-Nath equations

In the semiclassical limit the dimensions of RN matrix defined by Equation (10) are infinite and numerical diagonalisation becomes impossible. Dingle and Morgan [11, 12] (1967a, 1967b) (see appendix of Berry [3] (1966)) and independently Yakovlev [22] (1997), have given a WKB-type solution for the *continued* RN equations accurate in the large Λ limit. The idea is to capture the very fast oscillation of the Bloch wave (see Figures 3–7) with the exponential of a slowly varying function. To this end one replaces the discrete variable n with the continuous one y

$$y \equiv \frac{n}{\sqrt{\Lambda}} \quad (12)$$

so that when $n \rightarrow n + 1$, then $y \rightarrow y + (\sqrt{\Lambda})^{-1}$ and the discrete amplitudes become continuous functions of y , $B_n \rightarrow B(y)$. Defining the rescaled eigenvalue

$$\beta \equiv \frac{E}{\Lambda} \quad (13)$$

the stationary RN equation (10) becomes

$$(\beta - y^2)B(y) + \frac{1}{2} \left[B(y + (\sqrt{\Lambda})^{-1}) + B(y - (\sqrt{\Lambda})^{-1}) \right] = 0. \quad (14)$$

Following Berry [3] (1966), let

$$B(y) = e^{iS(y)} \quad (15)$$

where the suggestively named $S(y)$ is analogous to an action. Taylor expanding $S(y + (\sqrt{\Lambda})^{-1})$ and $S(y - (\sqrt{\Lambda})^{-1})$ gives a differential equation of infinite order

$$\cos \left(S^i + \frac{S^{iii}}{6} + \dots \right) = (y^2 - \beta) e^{-i(S^{ii}/2 + S^{iv}/24 + \dots)} \quad (16)$$

where $S^m = (\sqrt{\Lambda})^{-m} \partial^m S / \partial y^m$ are assumed to be small quantities of order $(\sqrt{\Lambda})^{-m}$. Solving for the first derivative one has

$$\frac{1}{\sqrt{\Lambda}} \frac{\partial S}{\partial y} = \arccos \left[(y^2 - \beta) e^{-i(S^{ii}/2 + S^{iv}/24 + \dots)} \right] - \frac{S^{iii}}{6} - \dots \quad (17)$$

Expanding the right hand side (rhs) gives

$$\begin{aligned} \frac{1}{\sqrt{\Lambda}} \frac{\partial S}{\partial y} = & \arccos [y^2 - \beta] + i \frac{y^2 - \beta}{\sqrt{1 - (y^2 - \beta)^2}} \frac{S^{ii}}{2} - \frac{S^{iii}}{6} + i \frac{y^2 - \beta}{\sqrt{1 - (y^2 - \beta)^2}} \frac{S^{iv}}{24} \\ & + \frac{y^2 - \beta}{(1 - (y^2 - \beta)^2)^{3/2}} \frac{(S^{ii})^2}{8} + \dots \end{aligned} \quad (18)$$

which can be solved for S^i by iteration, yielding to second order

$$\frac{\partial S}{\partial y} \approx \sqrt{\Lambda} \arccos [y^2 - \beta] - i \frac{(y^2 - \beta)y}{1 - (y^2 - \beta)^2}. \quad (19)$$

The second term on the rhs can be integrated immediately so that the equation for S can be written

$$\begin{aligned} S & \approx \sqrt{\Lambda} \int \arccos [y^2 - \beta] dy - \frac{i}{4} \ln (1 - (y^2 - \beta)^2) \\ & \equiv \sqrt{\Lambda} S_0(y, \beta) - \frac{i}{4} \ln (1 - (y^2 - \beta)^2). \end{aligned} \quad (20)$$

Thus the continued eigenfunctions take the form (Berry [3](1966))

$$B(y) = e^{iS} \approx \frac{e^{i\sqrt{\Lambda} \int \arccos[y^2 - \beta] dy}}{(1 - (y^2 - \beta)^2)^{1/4}} = \frac{e^{i\sqrt{\Lambda} S_0(y, \beta)}}{(1 - (y^2 - \beta)^2)^{1/4}} \quad (21)$$

which resembles a WKB expression. In particular the denominator causes divergences at the turning-points

$$y = \pm\sqrt{\beta \pm 1}. \quad (22)$$

‘Bound’ solutions of Mathieu’s equation have energies lying between the top and bottom of the sinusoidal wells ($0 \leq E \leq V_0$) which translates into the bound eigenvalues occupying the range $-1 \leq \beta \leq 1$. This means that except for the situation when $\beta = 1$, *real* turning points for bound states are located at

$$y_{\pm} = \pm\sqrt{\beta + 1}. \quad (23)$$

‘Free’ states have energies above the wells. When E is sufficiently greater than V_0 it is easy to find WKB solutions of Mathieu’s equation directly in coordinate space (since they have no classical turning points and hence no divergences) rather than the momentum (Fourier) space used here. Similarly, it is also simple to find eigenfunctions in coordinate space when $\beta \approx -1$, since states near the very bottom of the wells are the most localised and see an essentially harmonic potential yielding hermite polynomials as solutions. The most interesting situation is for β lying close to $+1$. These are the states affected most by tunnelling between the wells and will be examined in sections 10–19.

The remaining ‘action’ integral, giving the phase of the WKB solution (21), can be calculated using the positive turning point $y_+ = \sqrt{\beta + 1}$ as the lower limit (i.e. the zero or reference point of the phase)

$$\begin{aligned} S_0(y_+, y, \beta) &= \int_{\sqrt{\beta+1}}^y \arccos[y'^2 - \beta] dy' \\ &= y \arccos[y^2 - \beta] - 2\sqrt{1 + \beta} E\left(\frac{1}{2} \arccos[y^2 - \beta] \middle| \frac{2}{1 + \beta}\right) \end{aligned} \quad (24)$$

where $E(\phi|m) = \int_0^\phi \sqrt{1 - m \sin^2 \theta} d\theta$ is the incomplete elliptic integral of the second kind, see Gradshteyn and Ryzhik [14] (1965). This expression for the phase is valid for $0 \leq y \leq \sqrt{\beta + 1}$. For perpendicular incidence the phase is symmetrical about $y = 0$, and so only this half-range is required. For values of y greater than $\sqrt{\beta + 1}$ the phase is purely imaginary, but with care (24) still gives the correct answer.

4. Single and double wells in momentum space

Whilst it is useful to think of Equation (21) as a WKB type expression it does have some unusual features due to its unorthodox derivation from a difference equation. Usually, for the Schrödinger equation

$$\frac{d^2\psi(q)}{dq^2} + \frac{p^2(q)}{\hbar^2}\psi(q) = 0 \quad (25)$$

where $p(q)$ is the momentum, one has the approximate WKB solution (Berry and Mount [5] (1972)), valid for small \hbar as long as one is not too close to the turning-points ($p(q) = 0$), of

$$\psi_{WKB}^{\pm} \equiv \frac{1}{\sqrt{p(q)}} \exp\left(\pm \frac{i}{\hbar} \int_0^q p(q') dq'\right) \quad (26)$$

where $+/-$ refers to right/left travelling waves. Equation (21) is actually for the *momentum space* wavefunction, but to keep the analogy with the familiar coordinate space WKB solution (26)

simple, Equation (21) will temporarily be treated as though it is a coordinate space expression. Thus, terms such as ‘momentum’ will refer to functions playing the analogous rôle to $p(q)$ above. In particular, what is peculiar about solution (21) is that the ‘momentum’ function appearing in the amplitude and phase are different. The two momenta,

$$p_1(y, \beta) \equiv \sqrt{1 - (y^2 - \beta)^2} \quad (27)$$

and

$$p_2(y, \beta) \equiv \arccos [y^2 - \beta] \quad (28)$$

coincide for $\beta \rightarrow -1$, but are quite different when $\beta \rightarrow 1$. Examining Figure 2 one notes that the momentum appearing in the phase, p_2 , is that exhibited by a particle in a simple well. The amplitude momentum, p_1 , however, corresponds to a particle in a double well—although, except for values of β greater than one, the particle has enough energy to move between the two wells. It is the classical turning-point structure that is of paramount importance (see Berry and Mount [5] (1972) for a review of the WKB procedure), so the different local values of the two momenta give similar behaviour when $\beta < 1$. However, as the turning-point structure of p_1 changes from two to four, at $\beta = 1$, one can expect a qualitatively different response.

This retrospective observation, that the RN equations in some sense describe a wave in a single/double well, will be exploited to find uniform solutions in section 7. If one were to treat Mathieu’s equation directly in coordinate space then the infinite number of turning points due to the periodic well structure of the potential make a semiclassical analysis more complicated, see Berry [4] (1971), so no uniform solution has been previously given.

5. The Bohr-Sommerfeld condition

For states in a well, single-valuedness of the wavefunction dictates that only certain discrete energies are allowed. These eigenvalues/characteristic numbers ensure the integral of the WKB phase, Equation (24), from one turning-point to the other (that is, the integral across the classically accessible part of the potential well), correctly matches the oscillating part of the WKB wavefunction onto (asymptotically) exponentially decaying parts of the wavefunction (that tunnel into the classically forbidden sides of the well).

The action right across the well, given by setting the upper integration limit of Equation (24) equal to $-\sqrt{\beta + 1}$, is also equal to, for perpendicular incidence, twice the value found by integrating only halfway, to the midpoint of the well at $y = 0$,

$$2S_0(y_+, 0, \beta) = -4\sqrt{1 + \beta} \operatorname{E} \left(\frac{1}{2} \arccos [-\beta] \middle| \frac{2}{1 + \beta} \right). \quad (29)$$

The Bohr-Sommerfeld condition then states

$$2\sqrt{\Lambda} |S_0(y_+, 0, \beta^j)| = \left(j + \frac{1}{2} \right) \pi, \quad j = 0, 1, 2, 3 \dots \quad (30)$$

The root of this equation (which must be found numerically) for each value of j gives the β^j eigenvalues. This expression also gives the number of bound states that exist once a value for Λ has been chosen. The term ‘bound’ here refers to the coordinate space states that energetically lie below the maxima of the sinusoidal potential. In momentum space all the states are trapped in a well. The most energetic bound state, labelled j_{\max} , has the value of β which is closest to one. When Λ is large the eigenvalues lie very close to each other, and in particular,

$$\lim_{\Lambda \rightarrow \infty} \beta^{j_{\max}} = 1 \quad (31)$$

and since $\operatorname{E} \left(\frac{\pi}{2} \middle| 1 \right) = 1$, then

$$\lim_{\Lambda \rightarrow \infty} j_{\max} = \frac{4\sqrt{\Lambda}\sqrt{2}}{\pi} - \frac{1}{2}. \quad (32)$$

Although this gives the total number of possible bound states, not all of them are necessarily used in the superposition which gives the diffracted wavefunction. The superposition coefficients, which establish the relative contribution of each Bloch wave to the total wavefunction, are determined from the overlap of the initial plane wave ($A_n(\zeta = 0) = \delta_{n0}$) with the Bloch waves. The overlap integral is tricky in coordinate space but trivial in momentum space. Each coefficient is given by the value of the corresponding Bloch wave at $y = n = 0$. Thus only the even Bloch waves are excited.

6. Real eigenvectors and normalisation

Since the stationary RN equation (14) is real it is always possible to find real solutions. This is achieved by constructing a superposition of the two independent solutions: the right and left travelling waves of Equation (26), which correctly matches the exponential decay into the classically forbidden regions (Berry and Mount [5] (1972)). In the classically allowed region the single well has the solution

$$B_{\text{WKB}}(y, \beta) = \frac{\mathcal{N}(\beta)}{(1 - (y^2 - \beta)^2)^{1/4}} \cos\left(\sqrt{\Lambda} S_0(y_+, y, \beta) + \frac{\pi}{4}\right) \quad (33)$$

where S_0 is given by Equation (24), and $\mathcal{N}(\beta)$ is a normalisation factor.

Normalisation of the discrete amplitudes B_n requires that $\sum_{n=-\infty}^{\infty} |B_n|^2 = 1$. When moving from a summation to the integration in the continuous variable y , care must be taken to include a factor of $\sqrt{\Lambda}$ which comes from the definition (12) of y , so that

$$\sum_{n=-\infty}^{\infty} \longrightarrow \int_{n=-\infty}^{\infty} dn \longrightarrow \sqrt{\Lambda} \int_{y=-\infty}^{\infty} dy. \quad (34)$$

And so normalising the eigenvectors requires the evaluation of

$$\int_{-\infty}^{\infty} \left| B_{\text{WKB}}^j(y) \right|^2 dy = 1. \quad (35)$$

When Λ becomes large the exponential decay of the wavefunction into the sides of the well becomes very rapid and one can ignore these contributions, so the integral is taken to be just that between the two turning-points of the classical motion. Further, the oscillation of the wavefunction is assumed to be very rapid (actually the normalisation factor derived in this way works well even for the ground state Bloch wave which has the shape of a Gaussian, i.e. is non-oscillatory) in comparison to the slow variation of the square of the amplitude. And so, without much loss of accuracy, the \cos^2 term can be replaced by its average value of one half. Although the amplitude diverges at the turning-points this divergence is still integrable. Thus, one takes

$$\frac{\sqrt{\Lambda}}{2} \int_{y_-}^{y_+} \frac{dy}{\sqrt{1 - (y^2 - \beta)^2}} \approx \frac{1}{\mathcal{N}^2} \quad (36)$$

which gives

$$\mathcal{N}^2 \approx \frac{\sqrt{2}}{\sqrt{\Lambda} K\left(\frac{1+\beta}{2}\right)} \quad (37)$$

where $K(m) = \int_0^{\pi/2} (1 - m \sin^2 \theta)^{-1/2} d\theta$ is the complete elliptic integral of the first kind (Gradshteyn and Ryzhik [14] (1965)).

7. A Uniform approximation for the Raman-Nath equation

If the total diffracted wavefunction was calculated as a sum over the WKB Bloch waves then the diffraction pattern would contain spurious divergences at the turning points of each eigenfunction.

This problem can be avoided by using *uniform approximations* which give smooth and uniformly accurate eigenfunctions. A new, somewhat non-standard, uniform approximation for the momentum space Mathieu functions will be described in this and the following sections. To the best of the author's knowledge, a single global uniform approximation valid for all angles has not been previously given for the short-wavelength Mathieu functions. Existing uniform approximations are in coordinate space and are local to one or two turning points (e.g. the expansions due to R. Sips, see Abramowitz and Stegun (1964)) and so must be carefully joined together to give the complete solution.

Uniform approximations are based upon the idea that one can express the solutions to an unstudied differential equation in terms of those of a well known, studied, differential equation provided the two share a similar transition point (classical turning point) structure. A review of the uniform method can be found in Berry and Mount (1972). Since the method is central to the following calculations, it is reviewed in Appendix 1.

When constructing a uniform approximation to the continued stationary RN equation (14) it is not obvious what 'momentum' (the pretense of being in coordinate space rather than momentum space will continue to be maintained) function (i.e. $p(q) = \sqrt{E - V(q)}$ in Equation (26)) to use. The WKB-type solutions (21) continue to play an important rôle since they suggest using the 'momentum' functions p_1 and p_2 of Equations (27) and (28). It turns out that, as in the WKB case, matches to the actual momentum space Mathieu eigenfunctions are found when p_1 is used for the 'amplitude' part of the uniform approximation and p_2 for the 'phase' part. The mapping function should be based upon p_2 , which has the structure of a simple well. The simplest comparison equation for a well is

$$\frac{d^2\phi}{d\sigma^2} + (t - \sigma^2)\phi = 0. \quad (38)$$

The parameter t depends on the energy. The 'equivalent points' needed for Equation (107) are chosen to be the turning-points. This of course immediately satisfies the requirement that the zeros of Γ and χ correspond (See Appendix). Using (107), the integral across the well gives t , for then

$$\int_{y_-}^{y_+} \sqrt{\Lambda} p_2(y, \beta) dy \equiv -2\sqrt{\Lambda} S_0(y_+, 0, \beta) = \int_{-\sqrt{t}}^{+\sqrt{t}} \sqrt{t - \sigma^2} d\sigma = \frac{t\pi}{2} \quad (39)$$

where S_0 is given by Equation (24). Once t , which is a function of β , is known, the mapping function $\sigma(y)$ can be found from

$$\sqrt{\Lambda} S_0(y_+, y, \beta) = \int_{+\sqrt{t}}^{\sigma(y)} \sqrt{t - \sigma^2} d\sigma = \frac{t}{2} \left(\arcsin \left[\frac{\sigma}{\sqrt{t}} \right] + \frac{\sigma}{\sqrt{t}} \sqrt{1 - \frac{\sigma^2}{t}} - \frac{\pi}{2} \right). \quad (40)$$

Clearly this step must be executed by numerical root finding for each value of y which is required, i.e. those spaced at $1/\sqrt{\Lambda}$ intervals which are the angular positions of the diffracted beams.

There are two standard forms of the parabolic cylinder equation (Abramowitz and Stegun [1] (1964))

$$\frac{d^2\Theta}{dg^2} \mp \left(\frac{g^2}{4} \pm a \right) \Theta = 0. \quad (41)$$

The well Equation (38) corresponds to taking the upper signs. The simplest independent solutions to the parabolic cylinder equations are an even and an odd power series. However, combinations of these two power series lead to another two independent solutions, the Whittaker functions, which for large g decay or grow exponentially. The Whittaker functions have the correct properties to match the exponential tunnelling of the physical solution into the sides of the well. The Whittaker solutions to the well equation (38) are $D_{(t-1)/2}(\sigma\sqrt{2})$ and $D_{(t-1)/2}(-\sigma\sqrt{2})$. The standard

theory for the potential well uniform approximation would then predict the form of the Bloch wavefunction, correct for *all* y , to be

$$B(y) = \psi_{\text{uniform}} = \frac{1}{2} \mathcal{N} 2^{1/4} \left(\frac{2e}{t(\beta)} \right)^{t(\beta)/4} \left(\frac{d\sigma(y)}{dy} \right)^{-1/2} D_{(t(\beta)-1)/2} \left(-\sigma(y)\sqrt{2} \right) \quad (42)$$

and it is noted that for perpendicular incidence the choice of $+\sigma$ or $-\sigma$ makes no difference (only even eigenvectors are excited). The prefactors ensure that this expression has the same asymptotic behaviour when $\sigma, y \rightarrow \infty$ as the WKB solution (21).

Inserting the Bohr-Sommerfeld condition (30) into the equation for t , (39) above, gives the value of t which corresponds to the j^{th} eigenvalue

$$t = 2j + 1. \quad (43)$$

When the index of a Whittaker function is an integer, as here, it takes on the more familiar form

$$D_j(\sigma\sqrt{2}) = 2^{-j/2} H_j(\sigma) e^{-\sigma^2/2} \quad (44)$$

where H_j is a Hermite polynomial. However, for the higher Bloch waves (e.g. j greater than 20) it is more convenient to use, for reasons of speed of computation, the Airy function approximation to the Whittaker functions (see [1]).

8. Modifying the amplitude

The application of the uniform method to the WKB approximation to the RN equation as given above requires some adjustment. The existence of two momentum functions means the amplitude term of Equation (42),

$$\left(\frac{d\sigma(y)}{dy} \right)^{-1/2} = \left(\frac{t - \sigma^2}{\arccos^2[y^2 - \beta]} \right)^{1/4} \quad (45)$$

does not match the WKB behaviour (see Figure 2), since in that expression it is p_1 that appears in the amplitude. This disparity is removed by the substitution

$$\left(\frac{t - \sigma^2}{\arccos^2[y^2 - \beta]} \right)^{1/4} \longrightarrow \left(\frac{t - \sigma^2}{1 - (y^2 - \beta)^2} \right)^{1/4}. \quad (46)$$

The uniform approximation is formulated so that $\Gamma(\sigma)$ and $\chi(y)$ approach zero together so that the divergence inherent in the WKB solution is tamed. For the adjusted amplitude to give sensible answers this swapping of the momentum expressions must still lead to the correct behaviour at the turning-points. For $\beta < 1$, both p_1 and p_2 have the same zeros, and crucially for the uniform approximation they go to zero in the same way, namely as the square root of the distance from the zero.

L'Hôpital's rule can be used to find the limiting value of the amplitude (46) at the turning-point. After some calculation one finds

$$\lim_{y \rightarrow \sqrt{1+\beta}} \left[\frac{t - \sigma^2}{1 - (y^2 - \beta)^2} \right] = \lim_{y \rightarrow \sqrt{1+\beta}} \left[\frac{\Gamma}{p_1^2} \right] = \lim_{y \rightarrow \sqrt{1+\beta}} \left[\frac{\Gamma}{p_2^2} \right] = \left(\frac{\sqrt{t}}{2\sqrt{1+\beta}} \right)^{2/3}. \quad (47)$$

9. Comparison with the purely numerical calculation

Some pictures will now be used to compare the uniform method with the results of numerical diagonalisation (which can be taken as the 'exact' result). Figures 3–7 show a selection of Bloch waves with the uniform calculation shown as a solid line, though as before only the discrete values of y corresponding to the diffracted beams were used. The dots are the numerical data.

Figures 8–12 give the square of the modulus of the total wavefunction (i.e. the diffraction pattern), found by summing the Bloch waves, for a selection of depths (i.e. thicknesses of interaction

region). As mentioned at the end of section 5, the superposition coefficients in this sum are given by the value of the particular Bloch wave at $y = 0$. Only the bound states were used in both the numerical and uniform calculations, an approximation which is increasingly accurate in the classical limit. The intensity shown in Figure 8 clearly displays (the square of) an Airy function, which is well known to be the wavefunction associated with a fold caustic [6]. Caustics are the foci of the diffracted wavefield—classically they diverge and hence come to dominate the diffraction pattern in this limit. Figures 8–12 are the quantum equivalent of vertical slices through the classical ray trajectory picture, Figure 1b, of [8] (the depth, ζ , is the same classical unit denoted by x in that paper). The caustics are the envelopes of families of rays (each ray corresponds to a classical atom) which oscillate back and forth in the potential.

If the potential was harmonic then all the atoms would be focussed at $y = 0$ when $\zeta = m\pi$ ($m = 0, 1, 2, \dots$) and this behaviour can be seen in Figure 9 for $m = 1$. However, the anharmonicity of the sinusoidal potential means that the foci are imperfect and are smeared out into cusps with fold caustic arms. With increasing depth, successive oscillations of the atoms each introduce a new cusp which develops into a fold as it moves outwards through the pattern with increasing ζ . The result is an increasingly complicated interference pattern between successive Airy functions as shown in Figures 10–12, but usually with a few fringes of an outlying Airy function visible. The proliferation of caustics for increasing ζ is described only by dynamical diffraction and lies beyond the phase grating (or so-called ‘Raman-Nath’) approximation.

10. The problem of the separatrix

As has been already been noted, when the eigenvalue β approaches 1 the solution to the RN equation changes its nature. Classically, the motion of a particle in the sinusoidal potential goes from being trapped in a single well (libration) to being free (rotation) when its energy passes through the separatrix at $\beta = 1$ from below. At the same time the number of turning points of the ‘momentum’ function p_1 jumps from two to four and in so doing p_1 becomes qualitatively different from p_2 —as apparent from Figure 2 when the central dip breaks through the zero line. These new turning-points occur at

$$y = \pm\sqrt{\beta - 1}. \quad (48)$$

For small values of Λ the actual divergences due to these turning-points can fall between the diffracted orders and go unnoticed. As Λ is increased this is no longer the case and the divergences become clearly defined as the classical distribution emerges. It is emphasised that these divergences only affect those eigenvectors with eigenvalues close to the separatrix. Careful examination of the picture of the 200th eigenstate for $\Lambda = 12500$, reveals the first hint that the uniform approximation has a defect when β begins to approach 1. The remainder of this paper is concerned with these eigenstates close to the separatrix. Although only forming a small fraction of the total eigenstate sum giving the diffracted wavefunction, they are perhaps the most interesting states as they contain the very fine corrections due to tunnelling between the coordinate space potential wells in the semiclassical limit.

The uniform approximation used so far was not designed to handle the new turning-points. The momentum function p_2 used in the mapping relation (40) contains no information concerning the new turning-points. The amplitude and phase functions no longer act in concert. One way to proceed is by a transformation upon the RN equation which results in both the momentum functions have turning-points at $y = \sqrt{\beta - 1}$. Defining

$$B_n = (-1)^n C_n \quad (49)$$

the stationary R-N equation (14) becomes

$$(y^2 - \beta)C_n + \frac{1}{2}(C_{n+1} + C_{n-1}) = 0. \quad (50)$$

from which one obtains an altered action

$$\frac{\partial S}{\partial y} = \sqrt{\Lambda} \arccos [\beta - y^2] + i \frac{(\beta - y^2)y}{1 - (\beta - y^2)^2} \quad (51)$$

leading to the WKB formula

$$C(y) = \frac{e^{\pm i \sqrt{\Lambda} \int \arccos [\beta - y^2] dy}}{(1 - (y^2 - \beta)^2)^{1/4}} = \frac{e^{\pm i \sqrt{\Lambda} \bar{S}_0(y, \beta)}}{(1 - (y^2 - \beta)^2)^{1/4}}. \quad (52)$$

The amplitude is the same as before, giving the two sets of turning-points, but the phase momentum

$$\bar{p}_2(y, \beta) = \arccos [\beta - y^2] \quad (53)$$

now has its turning-points at $y = \pm \sqrt{\beta - 1}$ as promised. The cost is the loss of the turning-points at $y = \pm \sqrt{\beta + 1}$. The effect of the transformation is in swapping the rôles of inner and outer turning-points. Figure 13 shows that whereas p_2 has the momentum profile for a well, \bar{p}_2 has that of barrier which the particle has enough energy to surmount.

Since the phase momentum functions p_2 and \bar{p}_2 only describe one set of turning-points each, one is forced into employing two separate transitional uniform approximations for each eigenfunction when one is close to the separatrix. One transitional approximation covers the inner turning points and the other the outer. Both are valid in the intermediate region where they smoothly join.

11. The parabolic barrier equation

The inner turning-points require a transitional approximation for a (smooth) potential barrier. A suitable comparison equation is

$$\frac{d^2 \phi}{d\sigma^2} + (t + \sigma^2) \phi = 0. \quad (54)$$

For $t > 0$, the Bloch states are more energetic than the central potential barrier, and classically one has transmission above the barrier. This is referred to as the *underdense* case. Making the change of variables

$$t = i\bar{t} \quad (55)$$

$$\sigma = \frac{\bar{\sigma}}{\sqrt{2}} e^{i\pi/4} \quad (56)$$

one is lead back to the equation

$$\frac{d^2 \phi}{d\bar{\sigma}^2} - \left(\frac{\bar{t}}{2} + \frac{\bar{\sigma}^2}{4} \right) \phi = 0 \quad (57)$$

which is the same as the first (upper sign) parabolic cylinder equation (41) when the identifications $g = \bar{\sigma}$ and $a = \bar{t}/2$ are made.

The appropriate solutions for the barrier top are not the Whitakker functions since a parabolic barrier does not give an exponentially decaying wavefunction for large g . Instead, for a barrier, the basic even and odd power series solutions, which will be referred to as $\Theta_1(a, g)$ and $\Theta_2(a, g)$ respectively, are the correct choice. Close to the barrier top a is small and the power series solutions are most conveniently expressed in terms of the confluent hypergeometric functions

$$\Theta_1(a, g) = e^{-g^2/4} {}_1F_1 \left(\frac{a}{2} + \frac{1}{4}; \frac{1}{2}; \frac{g^2}{2} \right) \quad (58)$$

$$\Theta_2(a, g) = g e^{-g^2/4} {}_1F_1 \left(\frac{a}{2} + \frac{3}{4}; \frac{3}{2}; \frac{g^2}{2} \right). \quad (59)$$

As discussed previously, the boundary conditions mean that only even eigenfunctions are of interest here. Thus, the underdense inner turning point transitional approximation will be based upon the even power series

$$\Theta_1 \left(-i\frac{t}{2}, \sqrt{2}\sigma e^{-i\pi/4} \right). \quad (60)$$

12. The action for an underdense barrier

The underdense barrier does not induce any real turning-points (though of course the proximity of the turning-points to the real axis gives the deviation of the WKB amplitude from the true value) so the natural choice of reference point from which to integrate the phase is $y = \sigma = 0$. One finds

$$\begin{aligned} \bar{S}_0(0, y, \beta) &= \int_0^y \arccos [\beta - y'^2] dy' \\ &= y \arccos [\beta - y^2] + 2i\sqrt{1-\beta} E \left(\frac{1}{2} \arccos [\beta - y^2] \middle| \frac{2}{1-\beta} \right) \\ &\quad - E \left(\frac{1}{2} \arccos [\beta] \middle| \frac{2}{1-\beta} \right). \end{aligned} \quad (61)$$

Although it appears that this action contains an imaginary piece this is actually not the case. Strictly, the well known transformations (see [1]) should be applied to the elliptic functions so that their parameters lie between zero and one (the parameter used above tends to infinity as $\beta \rightarrow 1$). When this is done the action \bar{S}_0 is explicitly real. However, the transformations produce more complicated expressions so will not be applied here.

To find the value of t , which was previously given by the integral across the well, one must now integrate up the imaginary axis between the points

$$y_{\pm} = \pm\sqrt{\beta-1} = \pm i\sqrt{1-\beta}. \quad (62)$$

The equivalent points for the underdense barrier comparison equation (54) are

$$\sigma = \pm i\sqrt{t}. \quad (63)$$

Letting $y = iv$ and $\sigma = i\varsigma$, t is implicitly given by

$$2i\sqrt{\Lambda} \int_0^{\sqrt{1-\beta}} \arccos [\beta + v^2] dv = 2i \int_0^{\sqrt{t}} \sqrt{t^2 - \varsigma^2} d\varsigma \quad (64)$$

which, in a similar to fashion to before, results in the condition

$$4\sqrt{\Lambda}\sqrt{1-\beta}E \left(\frac{1}{2} \arccos [\beta] \middle| \frac{2}{1-\beta} \right) = \frac{t\pi}{2}. \quad (65)$$

The mapping function between σ and y implicitly giving $\sigma(y)$ is

$$\sqrt{\Lambda}\bar{S}_0(0, y, \beta) = \int_0^\sigma \sqrt{t + \sigma^2} d\sigma = \frac{t}{2} \left(\operatorname{arccosh} \left[\sqrt{1 + \frac{\sigma^2}{t}} \right] + \frac{\sigma}{\sqrt{t}} \sqrt{1 + \frac{\sigma^2}{t}} \right) \quad (66)$$

which, together with the value of t , gives the transitional approximation to the wavefunction

$$\begin{aligned} B(y) &= (-1)^n C(y) = (-1)^n \psi_{\text{transitional}} \\ &\propto (-1)^n \left(\frac{t + \sigma^2}{1 - (y^2 - \beta)^2} \right)^{1/4} e^{i\sigma^2/2} {}_1F_1 \left(-i\frac{t}{4} + \frac{1}{4}; \frac{1}{2}; -i\sigma^2 \right). \end{aligned} \quad (67)$$

This is a real function for real t and σ , which is valid from $y = 0$ and almost all the way to the outer turning-point, breaking down close to it because it is only set up to deal with the inner turning-point. The constant of proportionality will now be obtained by matching the asymptotic behaviour of this function to the WKB solution somewhere between the two transition points.

13. The asymptotics of the barrier transitional approximation

The confluent hypergeometric function has well known asymptotics. When $|\sigma|$ is large

$$\begin{aligned} {}_1F_1\left(-i\frac{t}{4}+\frac{1}{4};\frac{1}{2};-i\sigma^2\right) \\ = \frac{\Gamma\left(\frac{1}{2}\right)}{\Gamma\left(\frac{1}{4}+i\frac{t}{4}\right)}e^{-i\pi(-it+1)/4}(-i\sigma^2)^{(it-1)/4}\left(1+\frac{(it^2-4t-3i)}{16\sigma^2}+\mathcal{O}\left(\frac{1}{\sigma^4}\right)\right) \\ + \frac{\Gamma\left(\frac{1}{2}\right)}{\Gamma\left(\frac{1}{4}-i\frac{t}{4}\right)}e^{-i\sigma^2}(-i\sigma^2)^{-(it+1)/4}\left(1+\frac{(-it^2-4t+3i)}{16\sigma^2}+\mathcal{O}\left(\frac{1}{\sigma^4}\right)\right) \end{aligned} \quad (68)$$

where Γ is the Gamma (factorial) function. So

$$\begin{aligned} \Theta_1\left(-i\frac{t}{2},\sqrt{2}\sigma e^{-i\pi/4}\right) &= e^{i\sigma^2/2} {}_1F_1\left(-i\frac{t}{4}+\frac{1}{4};\frac{1}{2};-i\sigma^2\right) \\ &\sim \Gamma\left(\frac{1}{2}\right)(-i\sigma^2)^{-1/4}\left(e^{-\pi(t+i)/4}e^{i\sigma^2/2}\frac{(-i\sigma^2)^{it/4}}{\Gamma\left(\frac{1}{4}+i\frac{t}{4}\right)}e^{\ln[1+(it^2-4t-3i)/(16\sigma^2)]}\right. \\ &\quad \left.+ e^{-i\sigma^2/2}\frac{(-i\sigma^2)^{-it/4}}{\Gamma\left(\frac{1}{4}-i\frac{t}{4}\right)}e^{\ln[1-(it^2+4t-3i)/(16\sigma^2)]}\right) \end{aligned} \quad (69)$$

which conveniently reduces to

$$\begin{aligned} \Theta_1\left(-i\frac{t}{2},\sqrt{2}\sigma e^{-i\pi/4}\right) \\ \sim 2\frac{\Gamma\left(\frac{1}{2}\right)}{|\Gamma\left(\frac{1}{4}+i\frac{t}{4}\right)|}\sigma^{-1/2}e^{-\pi t/8-t/(4\sigma^2)}\cos\left(\frac{t}{2}\ln\sigma+\frac{\sigma^2}{2}-\text{Arg}\left[\Gamma\left(\frac{1}{4}+i\frac{t}{4}\right)\right]-\frac{\pi}{8}+\mathcal{O}\left(\frac{1}{\sigma^4}\right)\right). \end{aligned} \quad (70)$$

When Λ is large enough σ quickly takes on large values for even modest sizes of y , and so the confluent hypergeometric function attains its asymptotic form in the region between the inner and outer turning-points. It may then be compared to the WKB solution (52) for the transformed RN equation. The left and right travelling WKB waves (52) are combined to give a real solution

$$B_{\text{barrier}}(y) = \frac{\mathcal{N}}{(1-(y^2-\beta)^2)^{1/4}}\cos\left(\sqrt{\Lambda}\bar{S}_0(0,y,\beta)+\mu(\beta)+\sqrt{\Lambda}\pi y\right) \quad (71)$$

where the $(-1)^n$ factor has been incorporated into the phase of the cosine as $\sqrt{\Lambda}\pi y$. To enable a direct comparison, the phase of the cosine of Equation (70) should also be augmented by the same quantity. The real phase angle $\mu(\beta)$ for this parabolic barrier approximation (which for a simple first order turning-point, due to a linear potential, is equal to $\pi/4$) will this time be determined by consistency with the asymptotic solution (70). In order for a comparison to be made, the action $\bar{S}_0(0,y,\beta)$ appearing in the WKB solution must be written in terms of (σ,t) , which is accomplished through Equation (66). Expanding the rhs of (66) for $\sigma \gg t$, one has

$$\frac{t}{2}\left(\text{arccosh}\left[\sqrt{1+\frac{\sigma^2}{t}}\right]+\frac{\sigma}{\sqrt{t}}\sqrt{1+\frac{\sigma^2}{t}}\right)\sim\frac{t}{2}\ln\sigma-\frac{t}{4}\ln t+\frac{t}{2}\ln 2+\frac{\sigma^2}{2}+\frac{t}{4}+\mathcal{O}\left(\frac{t^2}{\sigma^2}\right) \quad (72)$$

implying that

$$\mu = \frac{t}{4} \ln t - \frac{t}{2} \ln 2 - \frac{t}{4} - \text{Arg} \left[\Gamma \left(\frac{1}{4} + i \frac{t}{4} \right) \right] - \frac{\pi}{8}. \quad (73)$$

Figure 14 demonstrates that this expression for μ is correct by comparing the WKB solution (71) containing it, with the fully numerical calculation. The value of Λ is reasonably small so the WKB solution diverges only very slightly from the correct value.

The exact solution to the parabolic cylinder equation has thus contributed to the evaluation of the phase of the WKB solution. On the other hand, the WKB solution indicates the necessary modifications needed for the amplitude of the parabolic cylinder equation so that it becomes the correct transitional solution to the particular problem being dealt with. Equating the amplitudes of Equations (70) and (71), one finds Equation (67) can now be updated to read

$$B_{\text{barrier}}(y) = (-1)^n \mathcal{N} \frac{|\Gamma(\frac{1}{4} + i \frac{t}{4})| e^{\pi t/8}}{2\Gamma(\frac{1}{2})} \left(\frac{t + \sigma^2}{1 - (y^2 - \beta)^2} \right)^{1/4} e^{i\sigma^2/2} {}_1F_1 \left(-i \frac{t}{4} + \frac{1}{4}; \frac{1}{2}; -i\sigma^2 \right). \quad (74)$$

The parabolic transitional approximation is compared to the fully numerical result in Figure 15 A). At first sight the match does not seem too good. The reason is that the normalisation uses the WKB amplitude factor, which diverges at the turning-points. When there are only the outer turning-points this method seems to work (see Figures 3-6) since the divergences are narrow enough to not produce too significant a contribution. However, the appearance of the inner turning-point divergences close to the separatrix energy now means the normalisation factor is significantly over estimating the magnitude of the wavefunction, and thus reduces the magnitude too much as shown. With relatively little effort one can numerically normalise the uniformly calculated eigenvectors by summing the discrete amplitudes, and when this is carried out the match, shown in Figure 15 B), is exceedingly good. This illustrates that it is only the normalising factor which is at fault. Figure 15 B) further illustrates that the barrier transitional approximation, Equation (74), is correct nearly throughout the entire momentum range—only breaking down close to the *outer* turning-point.

14. Calculation of the eigenvalues close to the separatrix—a modified Bohr-Sommerfeld rule

There is a slight complication to the calculation of the allowed values of β close to the separatrix which needs to be highlighted. When comparing the values of β obtained by the numerical diagonalisation technique with those obtained via Equation (30), the two differ when β grows very close to one. Somehow the derivation of the basic WKB solution (21) has failed to capture the full behaviour of the p_2 function—perhaps it should now after all contain two turning-points, not one, and so match the structure of the amplitude p_1 term? (Implying the transformation (49) of the phase momentum is more than a device.) From the point of view of the eigenvectors this can be overcome by replacing the previous single uniform approximation with two transitional approximations when β approaches one; the parabolic transitional approximation to cover the inner turning-point, and an Airy function approximation for the outer turning-point (since this remains a simple first order turning-point). However, to calculate the allowed values of the action which corresponds to the bound states, one needs some expression which is valid throughout the entire region which joins the two turning-points.

The general procedure for finding the action across a classically allowed region which separates two arbitrary types of turning-point employs two transitional approximations which are each valid at one end of the region, but these must be correctly joined. The quantised values of S , and hence β , are those which correctly match the two somewhere in the region of mutual validity.

The matching is most easily accomplished using the asymptotic forms for the two transitional approximations—which are of course their WKB approximations. In the region between the two

turning-points one thus has

$$\begin{aligned} \frac{1}{(1 - (y^2 - \beta)^2)^{1/4}} \cos \left(\sqrt{\Lambda} \bar{S}_0(0, y, \beta) + \mu(\beta) + \sqrt{\Lambda} \pi y \right) \\ = \frac{1}{(1 - (y^2 - \beta)^2)^{1/4}} \cos \left(\sqrt{\Lambda} S_0(\sqrt{1 + \beta}, y, \beta) + \frac{\pi}{4} \right) \end{aligned} \quad (75)$$

which implies that

$$\sqrt{\Lambda} \bar{S}_0(0, y, \beta) + \mu(\beta) + \sqrt{\Lambda} \pi y = \sqrt{\Lambda} S_0(\sqrt{1 + \beta}, y, \beta) + \frac{\pi}{4} \quad (76)$$

modulo 2π .

The method described above works in conventional situations with WKB expressions developed from (continuous) differential equations. Once again however, the approach has to be modified for the RN equation—whilst successful for the single well, as soon as the inner turning-points begin to approach the real axis even the matching of the two transitional approximations runs into trouble. The reason is that the continuous descriptions embodied above by Equation (75) do not match at all. Only when they are evaluated at the discrete points corresponding to diffracted beams do they match. The transformation (49) has produced two different equations whose continued WKB expressions only respect their common origin at the discrete level. It is then a surprise to find that at the correct (characteristic) values of β the discretely evaluated expressions on either side of Equation (75) are in perfect agreement for all y . Both are identical in each other's supposedly exclusive region of validity. This is rather curious, but the characteristic values of β , which one is able to predict by correctly matching the discrete points of the two WKB expressions, demonstrate that it is correct.

Due to the simultaneous validity for all y , the most sensible point to choose to match the two solutions is $y = 0$. The correct matching condition for even eigenstates becomes one of

$$\cos(\mu(\beta)) - \cos \left(\sqrt{\Lambda} S_0(y_+, 0, \beta) + \pi/4 \right) = 0 \quad (77)$$

$$\cos(\mu(\beta)) - \cos \left(\sqrt{\Lambda} S_0(y_+, 0, \beta) + 5\pi/4 \right) = 0 \quad (78)$$

the choice depending on whether the terminating Airy function has its peak above or below the y axis. In fact, successive even eigenstates alternate between the two conditions. When using (77) and (78), it is necessary to express μ , which is in the first instance a function of t , see Equation (73), as a function of β through the definition of t (Equation (65)). A further subtlety concerning the use of (77) and (78) is that close to each of the characteristic values there is another zero which does not correspond to an eigenvalue. The correct zeros are those through which the l.h.s. of Equations (77) and (78) have negative gradients. Table 1 compares the values of the top eight bound eigenvalues for $\Lambda = 12500$ as calculated by the different methods which have been outlined so far. Clearly the modified method gives excellent agreement with the true value and is superior to the regular Bohr-Sommerfeld scheme when close to the separatrix. The remaining error between the modified method and the true value becomes smaller as $\Lambda \rightarrow \infty$. This is further emphasised by the last entry on the table which is the last bound eigenvalue for $\Lambda = 250000$. The Bohr-Sommerfeld method predicts only 898 even bound states whereas the modified method accurately finds the value of the 900th.

15. The Airy transitional approximation

As has already been pointed out, to obtain the complete wavefunction correct for all y one must join the parabolic barrier approximation (74) to another transitional approximation which covers the outer, first order, turning-point. The comparison equation is given as an example in the

Appendix (Equation (109)), and choosing the reference point as $y = y_+ = \sqrt{1+\beta}$, the mapping function $\sigma(y)$ is given by

$$\sqrt{\Lambda} S_0(y_+, y, \beta) = \begin{cases} -\frac{2}{3} |\sigma|^{3/2} & \text{if } y \leq \sqrt{1+\beta}; \quad (\sigma < 0) \\ \frac{2}{3} i \sigma^{3/2} & \text{if } y > \sqrt{1+\beta}; \quad (\sigma > 0) \end{cases} \quad (79)$$

since the expression given for S_0 , Equation (24), is positive imaginary when $y > y_+$, and negative real when $y < y_+$.

The well known asymptotics of $\text{Ai}(\sigma)$ when $\sigma \gg 0$ are

$$\text{Ai}(\sigma) \sim \frac{1}{2\pi} \sigma^{-1/4} e^{-\frac{2}{3}\sigma^{3/2}} \quad (80)$$

and so the Airy transitional approximation becomes

$$\psi_{\text{transitional}} = B_{\text{Airy}}(y) = 2\pi \mathcal{N} \left(\frac{\sigma(y)}{1 - (y^2 - \beta)^2} \right)^{1/4} \text{Ai}(\sigma(y)). \quad (81)$$

16. The free eigenstates

As emphasised previously, ‘free’ is a description which refers to the (actual) configuration space situation of states having transverse energies greater than V_0 . In (actual) momentum space there are no free states, the classical bounding of the maximum being set by the initial transverse momentum plus whatever the atoms can extract from the potential—which depends on the (actual) configuration space point, but has a maximum of $\sqrt{2mV_0}$. Thus, even for $\beta > 1$, one expects caustics in (actual) momentum space. One sees why the free eigenstates are quantised and not continuous in energy. Somewhat perversely, the states which are free in (actual) configuration space, sit in a double well in (actual) momentum space, and so the central barrier is now *overdense*—meaning that classical transmission is forbidden. For perpendicular incidence, the free ‘states’ are classically inaccessible, so their contribution to the eigensum of states forming the total wavefunction is exponentially small.

For states with $\beta \gg 1$, the problem is most easily solved using the WKB technique in (actual) configuration space, since there are no turning-points to contend with. Constraining the discussion to perpendicular incidence means however that only those states with β a little greater than one need be calculated, so the ‘close to the separatrix’ treatment of the preceeding sections must be generalised to encompass $\beta > 1$. Since the essentials of the application of the uniform method to the Raman-Nath equation have already been conveyed, the following treatment is intended to be more of a ‘recipe’ than a detailed account.

The overdense barrier equation will be taken as

$$\frac{d^2 \phi}{d\sigma^2} + (\sigma^2 - t) \phi = 0 \quad (82)$$

with t a positive quantity. The connection with the parabolic cylinder equation (41) is made with the aid of the transformations

$$a = -i \frac{t}{2} \quad (83)$$

$$g = \sqrt{2\sigma} e^{i\pi/4}. \quad (84)$$

To remove any ambiguity regarding the phase momentum function p_2 for the barrier, it will be written as

$$\bar{p}_2 = \arccos[\beta - y^2] = \begin{cases} i \operatorname{arccosh}[\beta - y^2] & \text{if } 0 \leq y \leq \sqrt{\beta - 1} \\ \pi - \arccos[y^2 - \beta] & \text{if } \sqrt{\beta - 1} \leq y < \sqrt{1 + \beta} \end{cases} \quad (85)$$

where the central barrier lies between $\pm\sqrt{\beta-1}$. The actions generated from these momenta, using $y = \sqrt{\beta-1}$ as the reference point, are

$$\bar{S}_0^{y < \sqrt{\beta-1}}(\sqrt{\beta-1}, y, \beta) = i \left(y \operatorname{arccosh} [\beta - y^2] + 2i\sqrt{\beta-1} \operatorname{E} \left(\frac{1}{2} \operatorname{arccos} [\beta - y^2] \middle| \frac{2}{1-\beta} \right) \right) \quad (86)$$

and

$$\begin{aligned} \bar{S}_0^{y > \sqrt{\beta-1}}(\sqrt{\beta-1}, y, \beta) &= \pi y + 2\sqrt{\beta+1} \operatorname{E} \left(\frac{1}{2} \operatorname{arccos} [y^2 - \beta] \middle| \frac{2}{1+\beta} \right) \\ &\quad - 2\sqrt{\beta+1} \operatorname{E} \left(\frac{\pi}{2} \middle| \frac{2}{1+\beta} \right) - y \operatorname{arccos} [y^2 - \beta]. \end{aligned} \quad (87)$$

As before, the comparison equation (82) gives rise to the mapping function by setting

$$\bar{S}_0^{y < \sqrt{\beta-1}} = \int_{\sqrt{t}}^{\sigma} \sqrt{\sigma^2 - t} d\sigma = i \frac{t}{2} \left(\operatorname{arcsin} \left[\frac{\sigma}{\sqrt{t}} \right] + \frac{\sigma}{\sqrt{t}} \sqrt{1 - \frac{\sigma^2}{t}} - \frac{\pi}{2} \right) \quad (88)$$

and

$$\bar{S}_0^{y > \sqrt{\beta-1}} = \int_{\sqrt{t}}^{\sigma} \sqrt{\sigma^2 - t} d\sigma = \frac{t}{2} \left(\frac{\sigma^2}{t} \sqrt{1 - \frac{t}{\sigma^2}} - \operatorname{arccosh} \left[\frac{\sigma}{\sqrt{t}} \right] \right). \quad (89)$$

In particular, the ‘barrier integral’ which fixes the value of t once β is known, can this time be conducted along the real axis, and gives, using (86) and (88),

$$2i\sqrt{\Lambda}\sqrt{\beta-1} \operatorname{E} \left(\frac{1}{2} \operatorname{arccos} [\beta] \middle| \frac{2}{1-\beta} \right) = -\frac{t\pi}{4}. \quad (90)$$

The correct solution to the barrier equation is still the even power series

$$\Theta_1(a, g) = \Theta_1 \left(-i\frac{t}{2}, \sqrt{2}\sigma e^{i\pi/4} \right) \quad (91)$$

and so the transitional approximation for the overdense barrier becomes

$$\begin{aligned} B(y) &= (-1)^n C(y) = (-1)^n \psi_{\text{transitional}} \\ &\propto (-1)^n \left(\frac{\sigma^2 - t}{1 - (y^2 - \beta)^2} \right)^{1/4} e^{-i\sigma^2/2} {}_1F_1 \left(-i\frac{t}{4} + \frac{1}{4}; \frac{1}{2}; i\sigma^2 \right). \end{aligned} \quad (92)$$

17. Asymptotic matching to the overdense WKB expression

The transitional wavefunction differs by a few sign changes from the underdense case, and for large σ these produce the modified oscillatory behaviour:

$$\begin{aligned} &\Theta_1 \left(-i\frac{t}{2}, \sqrt{2}\sigma e^{i\pi/4} \right) \\ &\sim 2 \frac{\Gamma \left(\frac{1}{2} \right)}{\left| \Gamma \left(\frac{1}{4} + i\frac{t}{4} \right) \right|} \sigma^{-1/2} e^{\pi t/8 - t/(4\sigma^2)} \cos \left(\frac{t}{2} \ln \sigma - \frac{\sigma^2}{2} - \operatorname{Arg} \left[\Gamma \left(\frac{1}{4} + i\frac{t}{4} \right) \right] + \frac{\pi}{8} + \mathcal{O} \left(\frac{1}{\sigma^4} \right) \right). \end{aligned} \quad (93)$$

Expanding the rhs of Equation (89) for $\sigma \gg t$ gives

$$\frac{t}{2} \left(\frac{\sigma^2}{t} \sqrt{1 - \frac{t}{\sigma^2}} - \operatorname{arccosh} \left[\frac{\sigma}{\sqrt{t}} \right] \right) \sim -\frac{t}{2} \ln \sigma + \frac{t}{4} \ln t - \frac{t}{2} \ln 2 + \frac{\sigma^2}{2} - \frac{t}{4} \quad (94)$$

from which one deduces the unknown phase angle μ , appearing in the WKB approximation for the overdense barrier (see Equation (71)), to be

$$\mu = -\frac{t}{4} \ln t + \frac{t}{2} \ln 2 + \frac{t}{4} + \text{Arg} \left[\Gamma \left(\frac{1}{4} + i\frac{t}{4} \right) \right] - \frac{\pi}{8}. \quad (95)$$

18. The overdense eigenvalues

Once again μ can be successfully employed in the accurate determination of the eigenvalues β . Following the empirical observations from the underdense case, the WKB expression emanating from the outer turning-point and that from the inner turning-point are matched at a point y corresponding to one of the beams. This time the choice of $y = 0$ is not available since only the phase for the WKB approximation outside the barrier is known. The next most obvious choice is either the inner or outer turning-point since there the phase of the WKB expressions are simplest, but in general these classically determined points will not fall on a diffracted beam. Selecting a random beam, $y = m/\sqrt{\Lambda}$, with m an integer, giving of value y lying between the two turning-points, will suffice. The condition giving the permitted values of β for even eigenstates then alternates between

$$\begin{aligned} \cos \left(\sqrt{\Lambda} \bar{S}_0^{y > \sqrt{\beta-1}} \left(\sqrt{\beta-1}, \frac{m}{\sqrt{\Lambda}}, \beta \right) + \mu(\beta) + \sqrt{\Lambda} \pi \frac{m}{\sqrt{\Lambda}} \right) \\ - \cos \left(\sqrt{\Lambda} S_0 \left(\sqrt{1+\beta}, \frac{m}{\sqrt{\Lambda}}, \beta \right) + \frac{\pi}{4} \right) = 0 \end{aligned} \quad (96)$$

and

$$\begin{aligned} \cos \left(\sqrt{\Lambda} \bar{S}_0^{y > \sqrt{\beta-1}} \left(\sqrt{\beta-1}, \frac{m}{\sqrt{\Lambda}}, \beta \right) + \mu(\beta) + \sqrt{\Lambda} \pi \frac{m}{\sqrt{\Lambda}} \right) \\ - \cos \left(\sqrt{\Lambda} S_0 \left(\sqrt{1+\beta}, \frac{m}{\sqrt{\Lambda}}, \beta \right) + \frac{5\pi}{4} \right) = 0. \end{aligned} \quad (97)$$

Both of these equations have zeros which do not correspond to the eigenvalues, the correct ones being those for which gradient of the lhs' are positive (this is the opposite of the underdense case). As before, the accuracy which is achieved gives confidence to the method: for $\Lambda = 12500$ the first two free eigenvalues given by numerical diagonalisation are $\beta = 1.003356$ and $\beta = 1.012155$, for which this WKB matching technique gives $\beta = 1.003358$ and $\beta = 1.012156$ respectively.

19. The overdense eigenvectors

Knowing the value of β , one is in a position to calculate the transitional approximation to the overdense eigenvector

$$B_{\text{barrier}}(y) = (-1)^n \mathcal{N} \frac{\left| \Gamma \left(\frac{1}{4} + i\frac{t}{4} \right) \right| e^{-\pi t/8}}{2\Gamma \left(\frac{1}{2} \right)} \left(\frac{\sigma^2 - t}{1 - (y^2 - \beta)^2} \right)^{1/4} e^{-i\sigma^2/2} {}_1F_1 \left(-i\frac{t}{4} + \frac{1}{4}; \frac{1}{2}; i\sigma^2 \right). \quad (98)$$

The Airy function approximation for the outer turning-point remains the same as before. Figure 16 shows the first free eigenvector made up of the overdense barrier and Airy function approximations.

20. Conclusion

A new method for calculating the eigenvalues (characteristic values) and eigenvectors (Mathieu functions/Bloch waves) of the Mathieu equation in the short wavelength limit is given. The difficulties associated with the infinite number of turning points inherent in a periodic potential are circumvented by working in Fourier space with the Raman-Nath equation. Continued eigenvectors of this differential difference equation can be obtained via a WKB-type solution. The eigenvalues then follow from a simple Bohr-Sommerfeld relation.

Whilst the WKB solutions to the Raman-Nath equation still contain divergences, they reveal that the Raman-Nath equation can be interpreted as describing a wave in a double well potential, for which simple uniform approximations—solutions without singularities—exist in terms of the parabolic cylinder functions. There are three situations. Firstly, the ‘bound’ eigenstates lying below the separatrix in coordinate space lie above the central barrier in the double well in Fourier space and so a single uniform approximation in terms of Hermite polynomials suffices. Secondly, at or just below the coordinate space separatrix the eigenstates lie at or just above the central barrier in the double well in Fourier space, causing two new turning points to appear. A complete eigenfunction with no singularities can be constructed by smoothly sewing together two transitional approximations—a parabolic cylinder function and an Airy function (the double well in Fourier space is symmetrical so only two transitional approximations are required rather than three). Thirdly, above the coordinate space separatrix and consequently below the central barrier in Fourier space, the ‘free’ eigenstates are also given by matching a parabolic cylinder function and an Airy function. A prescription is given for the modification of the Bohr-Sommerfeld rule for the eigenvalues near the separatrix.

The Mathieu equation arises physically in the diffraction of waves by a sinusoidal potential. Knowing the eigenfunctions of the potential allows one to propagate the incident wave for any interaction distance and hence investigate dynamical diffraction phenomena which go beyond the phase-grating/Raman-Nath approximation, such as caustics (natural focussing). Semiclassically, the superposition of eigenfunctions giving the diffraction pattern due to an incident plane wave only contains an exponentially small contribution from the free eigenstates. However, as $\hbar \rightarrow 0$ ($\Lambda \rightarrow \infty$), even the number of ‘bound’ states become infinite. In a companion paper [17] it will be demonstrated that a Poisson resummation of the eigenfunction superposition produces a new series each term of which is associated with *classical paths* belonging to a different topological class. Furthermore, the number of terms required in this new sum depends linearly on the distance propagated through the potential (independent of the size of \hbar)—only a finite number of terms are required for finite propagation distances, and so is computationally superior to the original eigenfunction sum which requires an infinite number of terms in the $\hbar \rightarrow 0$ limit.

21. Acknowledgements

It is a pleasure to thank M.V. Berry, J.H. Hannay, W. Schleich and V.P. Yakovlev for numerous discussions and suggestions. I also thank the University of Bristol, U.K., for a studentship during which this work was undertaken.

Appendix: the method of uniform approximation

Details can be found in the review by Berry and Mount [5](1972). The objective is to obtain an approximate solution of the Helmholtz equation

$$\frac{d^2\psi(q)}{dq^2} + \chi(q)\psi(q) = 0 \quad (99)$$

in terms of solutions to one of the ‘studied’ equations, which will be written

$$\frac{d^2\phi(\sigma)}{d\sigma^2} + \Gamma(\sigma)\phi(\sigma) = 0. \quad (100)$$

The choice of studied equation is determined by $\Gamma(\sigma)$ (not *the* Gamma function) being in some way similar to $\chi(q)$. This similarity implies that $\phi(\sigma)$ also resembles the wavefunction $\psi(q)$, and “can be changed into it by stretching or contracting it a little and changing the amplitude a little”. And so $\psi(q)$ will be expressed in terms of $\phi(\sigma)$

$$\psi(q) = f(q)\phi(\sigma(q)). \quad (101)$$

Substitution of this definition into (99) and making use of (100) leaves

$$\frac{d^2f}{dq^2} + \chi f \phi - f \left(\frac{d\sigma}{dq} \right)^2 \Gamma \phi + \frac{d\phi}{d\sigma} \left(2 \frac{df}{dq} \frac{d\sigma}{dq} + f \frac{d^2\sigma}{dq^2} \right) = 0. \quad (102)$$

The amplitude $f(q)$ is as yet unspecified, so it is chosen to simplify (102) as much as possible. Putting

$$f = \left(\frac{d\sigma}{dq} \right)^{-\frac{1}{2}} \quad (103)$$

renders (102) into an equation purely for the ‘mapping function’ $\sigma(q)$

$$\chi = \left(\frac{d\sigma}{dq} \right)^2 \Gamma - \left(\frac{d\sigma}{dq} \right)^{\frac{1}{2}} \frac{d^2}{dq^2} \left(\frac{d\sigma}{dq} \right)^{-\frac{1}{2}} \quad (104)$$

which, when solved, gives σ as a function of q . If a good choice of comparison function $\Gamma(\sigma)$ has been made, then $\sigma(q)$ will be a slowly varying function and the second term on the rhs of (102) will be much smaller than the first. Clearly the criterion for this to be the case is

$$\epsilon(q) \equiv \left| \frac{1}{\chi(q)} \left(\frac{d\sigma}{dq} \right)^{\frac{1}{2}} \frac{d^2}{dq^2} \left(\frac{d\sigma}{dq} \right)^{-\frac{1}{2}} \right| \ll 1. \quad (105)$$

When this is satisfied, the mapping relation reduces to

$$\frac{d\sigma}{dq} \simeq \left(\frac{\chi(q)}{\Gamma(\sigma)} \right)^{\frac{1}{2}} \quad (106)$$

which through definition (103) also gives the amplitude f . Thus, by picking two points σ_0 and q_0 which are ‘equivalent’, one finds $\sigma(q)$ from

$$\int_{\sigma_0}^{\sigma} \sqrt{\pm \Gamma(\sigma)} d\sigma = \int_{q_0}^q \sqrt{\pm \chi(q)} dq \quad (107)$$

where the + or the – version can be chosen depending on the situation. The approximate solution to (99) is then

$$\psi(q) \simeq \left(\frac{\Gamma(\sigma(q))}{\chi(q)} \right)^{\frac{1}{4}} \phi(\sigma(q)). \quad (108)$$

In order for the comparison method to be viable, the mapping from q to σ must be one to one, which requires that $d\sigma/dq$ is never zero or infinite. Examining (106) this means that χ and Γ must not diverge—which is assumed to be the case—and more relevantly, their zeros must be made to correspond. The zeros are of course the turning-points, and so, as Berry and Mount emphasise, “in the semiclassical limit all problems are equivalent which have the same *classical turning-point structure*”.

Perhaps the best known example of the uniform approximation is for the lone, first order (that is, the potential is locally linear) turning-point leading to the comparison equation

$$\frac{d^2\sigma}{d\sigma^2} - \sigma\phi = 0 \tag{109}$$

whose solution is the Airy function, $\text{Ai}(\sigma)$. Many potentials of interest are linear close to the turning point. As one moves away from the turning point the Airy function can be smoothly matched onto a WKB solution which is capable of handling very complicated potentials provided there are no turning points. Used in this way, as a patch across the turning point, the Airy function constitutes what is sometimes referred to as a *transitional* approximation.

References

- [1] Abramowitz M and Stegun I A 1964 *Handbook of Mathematical Functions* (Washington, DC: National Bureau of Standards)
- [2] Adams C S, Sigel M and Mlynek J 1994 Atom optics *Phys. Rep.* **240** 143–210
- [3] Berry M V 1966 *The Diffraction of Light by Ultrasound* (New York: Academic)
- [4] Berry M V 1971 Diffraction in crystals at high energies *J. Phys. C: Solid State Phys.* **4** 697–722
- [5] Berry M V and Mount K E 1972 Semiclassical approximations in wave mechanics *Rep. Prog. Phys.* **35** 315–397
- [6] Berry M V 1981 *Les Houches Lecture Series* session XXXV, ed R. Balian *et al.* (Amsterdam: North Holland) pp 455–541
- [7] Berry M V and O’Dell D H J 1998 Diffraction by volume gratings with imaginary potentials *J. Phys. A: Math. Gen.* **31** 2093–2101
- [8] Berry M V and O’Dell D H J 1999 Ergodicity in wave-wave diffraction *J. Phys. A: Math. Gen.* **32** 3571–3582
- [9] Brillouin L 1921 *Annal Physique* **17** 103
- [10] Cohen-Tannoudji C, Dupont-Roc J and Grynberg G 1992 *Atom-Photon Interactions* (New York: Wiley-Interscience)
- [11] Dingle R B and Morgan G J 1967 WKB methods for difference equations I *Applied Scientific Research* **18** 221–237
- [12] Dingle R B and Morgan G J 1967 WKB methods for difference equations II *Applied Scientific Research* **18** 238–245
- [13] Gould P L, Ruff G A and Pritchard D E 1986 Diffraction of Atoms by Light: The Near-Resonant Kapitza-Dirac Effect *Phys. Rev. Lett.* **56** 827–830
- [14] Gradshteyn I S and Ryzhik I M 1965 *Table of Integrals, Series and Products* (New York: Academic)
- [15] Kazantsev A P, Surdutovich G I and Yakovlev V P 1991 *Mechanical Action of Light on Atoms* (Singapore: World Scientific)
- [16] O’Dell D H J 1999 *The Diffraction of Atoms by Light* (University of Bristol PhD thesis: unpublished)
- [17] O’Dell D H J 2001 to be published
- [18] Raman C V and Nagendra Nath N S 1935 The Diffraction of Light by High Frequency Sound Waves: Part I *Proc. Indian Acad. of Sci. A* **2** 406–412
- [19] Raman C V and Nagendra Nath N S 1936 The Diffraction of Light by High Frequency Sound Waves: Part IV *Proc. Indian Acad. of Sci. A* **3** 119–25
- [20] Rasel E M, Oberthaler M K, Batelaan H, Schmiedmayer J and Zeilinger A 1995 Atom Wave Interferometry with Diffraction Gratings of Light *Phys. Rev. Lett.* **75** 2633–2637
- [21] Sanders F H 1936 *Canadian J. Research* **A14** 158
- [22] Yakovlev V P 1997 private communication

Λ	j	fully numerical	single well calc.	modified calc.
12500	200	0.996129	0.996824	0.996131
	198	0.987197	0.987337	0.987199
	196	0.976711	0.976759	0.976713
	194	0.965430	0.965461	0.965432
	192	0.953575	0.953599	0.953578
	190	0.941244	0.941264	0.941247
	188	0.928498	0.928515	0.928499
	186	0.915379	0.915394	0.915381
250000	900	0.999954	—	0.999954

Table 1: The bound eigenvalues near the separatrix: comparison of numerical result with the standard Bohr-Sommerfeld condition for a well (30), and the modified conditions (77)–(78).

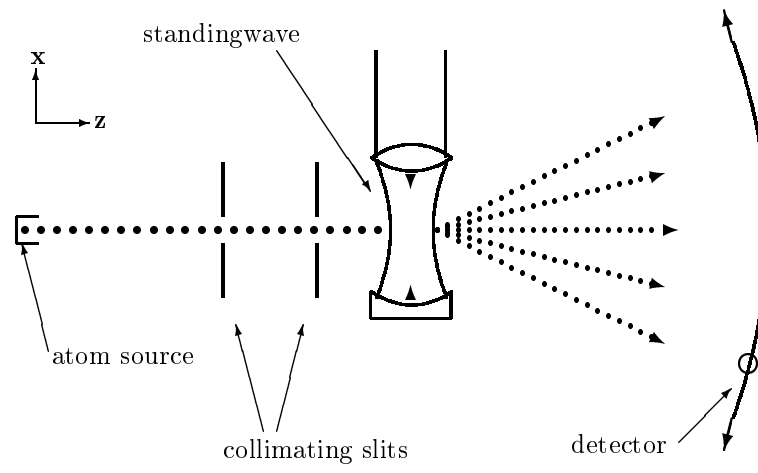


Figure 1: A typical experimental set-up used in the investigation of atomic diffraction.

)

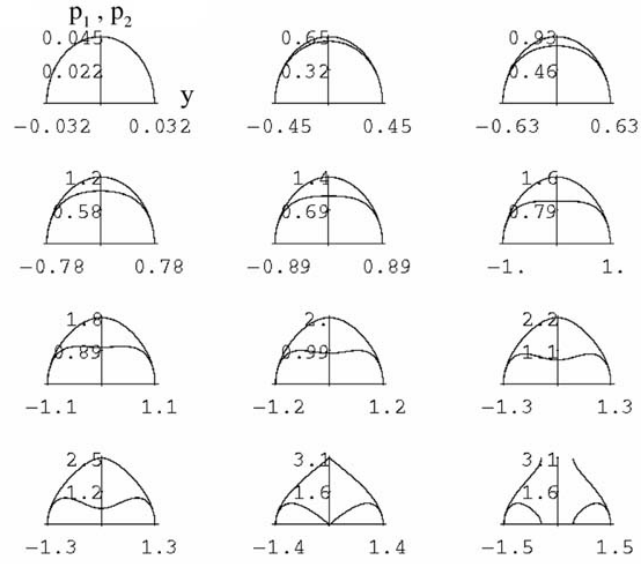


Figure 2: A series of plots showing the two momentum functions, p_1 and p_2 , as functions of y for different values of β . The top left has $\beta = -0.999$, each successive picture has β increasing by 0.2 until the bottom right which has $\beta = 1.201$. It is the p_1 curve that dips down to zero when $\beta = 1$.

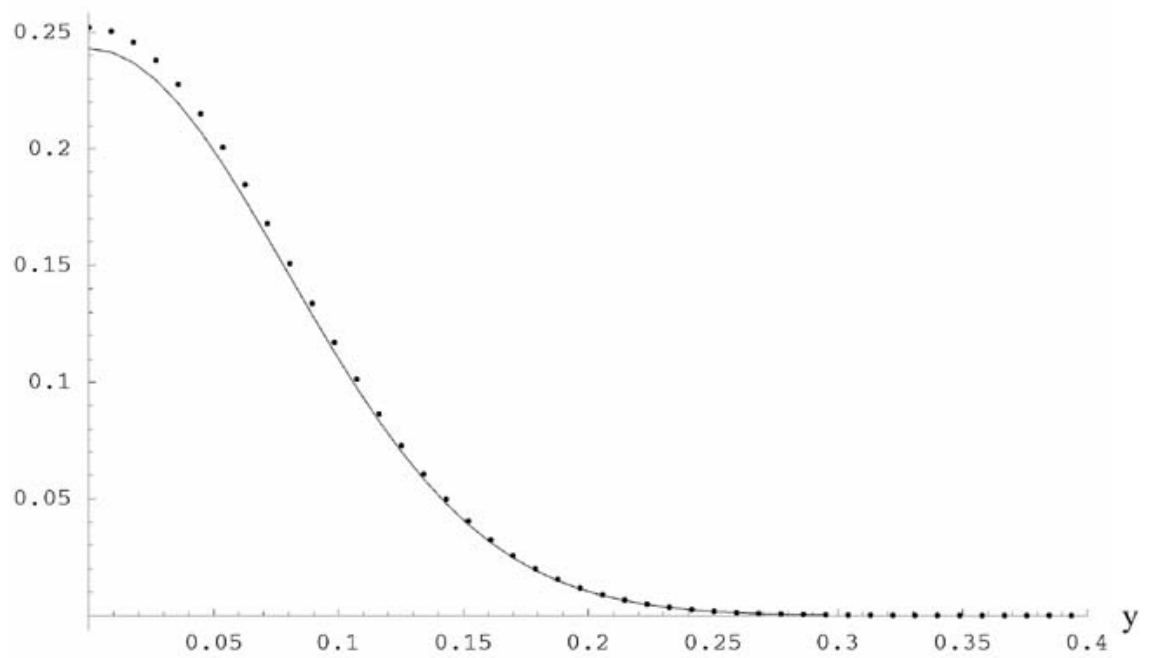


Figure 3: A comparison of the numerical (dots) 0th Bloch wave, out of 200 bound states, of the R-N matrix (10) for $\Lambda = 12500$, with its uniform approximation (solid line). $\beta = -0.9937$. Since the Bloch wave is symmetrical about $y = 0$, only the positive half is shown.

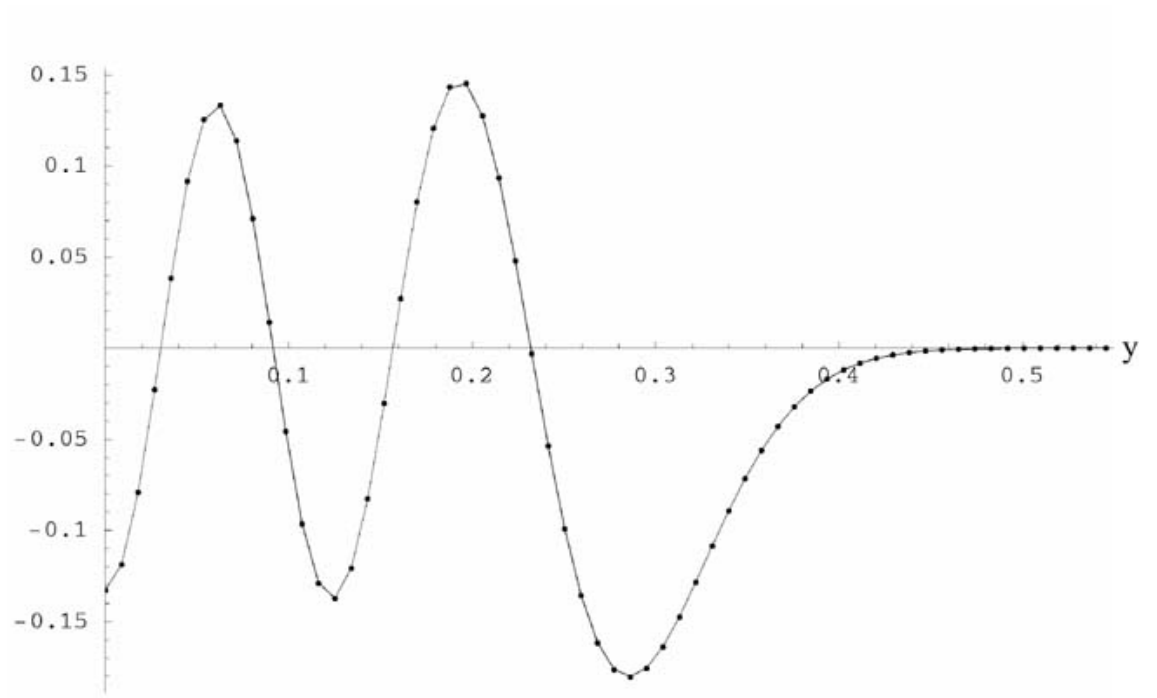


Figure 4: A comparison of the numerical (dots) 8th Bloch wave, out of 200 bound states, of the R-N matrix (10) for $\Lambda = 12500$, with its uniform approximation (solid line). $\beta = -0.8932$.

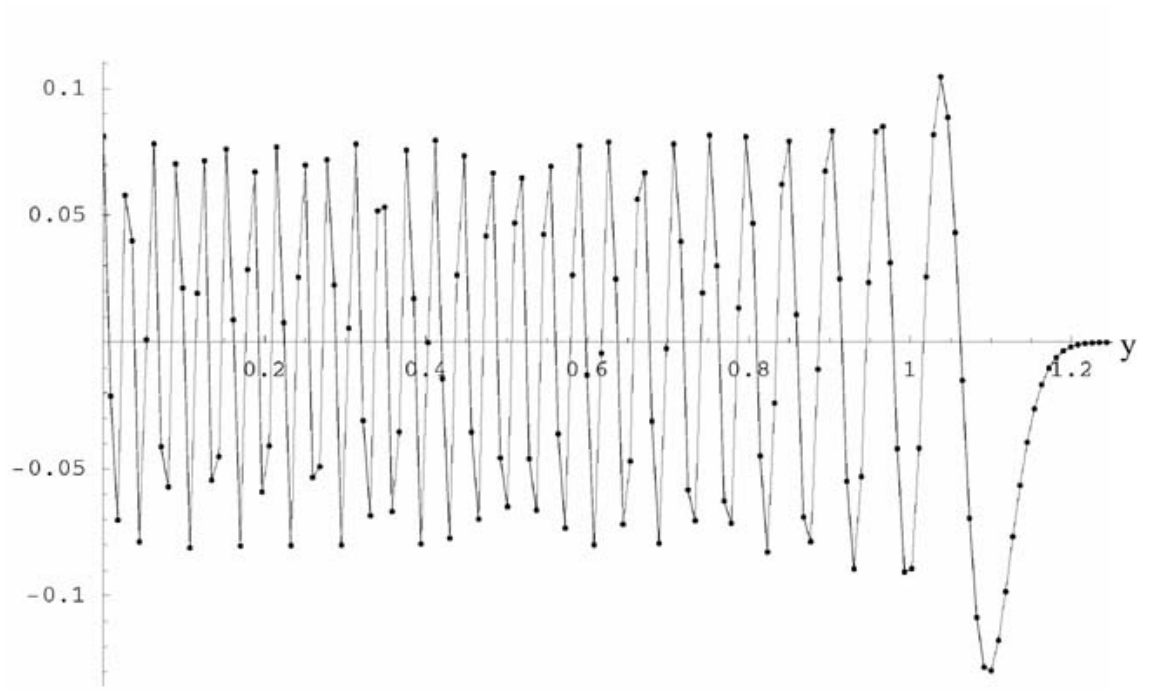


Figure 5: A comparison of the numerical (dots) 110th Bloch wave, out of 200 bound states, of the R-N matrix (10) for $\Lambda = 12500$, with its uniform approximation (solid line). $\beta = 0.2616$.

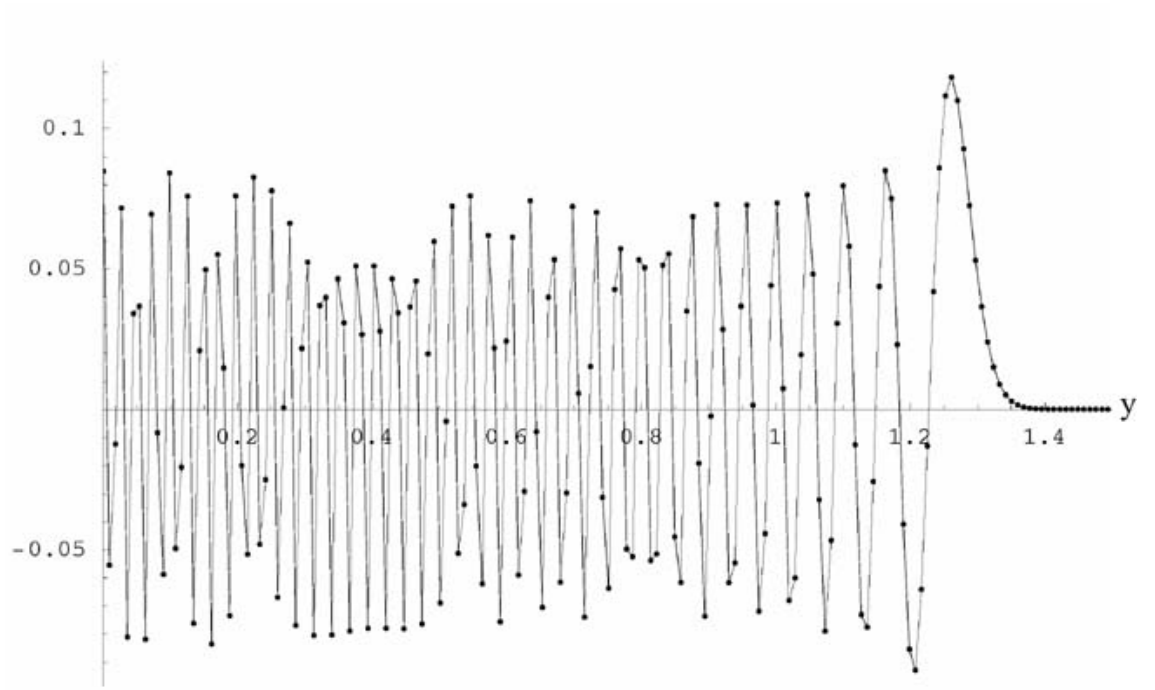


Figure 6: A comparison of the numerical (dots) 152nd Bloch wave, out of 200 bound states, of the R-N matrix (10) for $\Lambda = 12500$, with its uniform approximation (solid line). $\beta = 0.6532$.

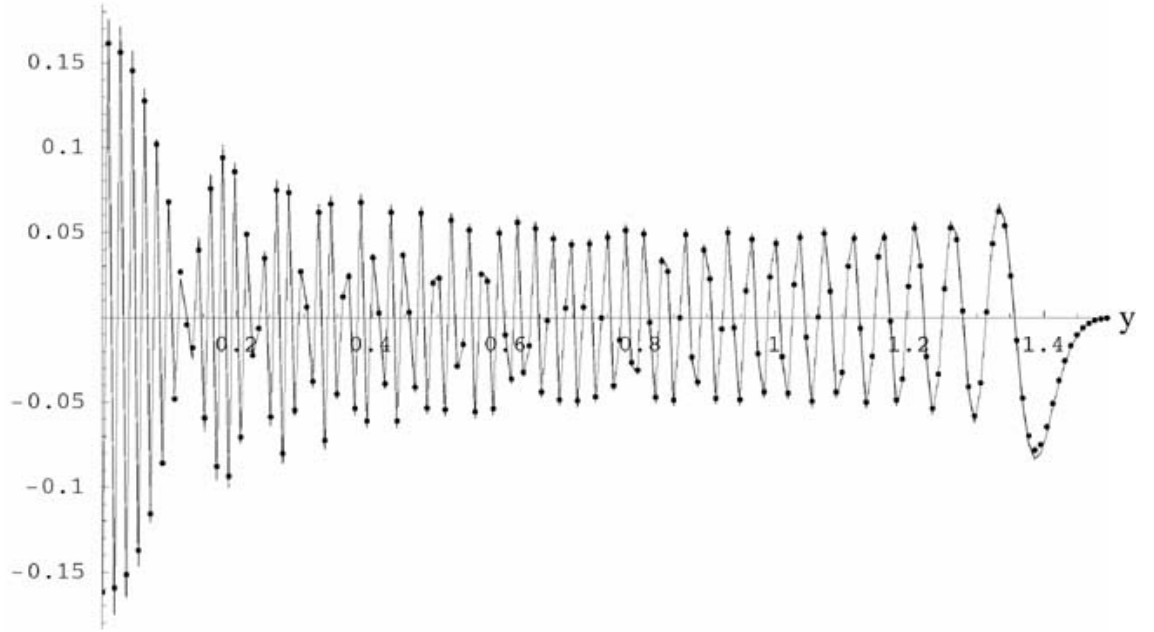


Figure 7: A comparison of the numerical (dots) 200th Bloch wave, out of 200 bound states, of the R-N matrix (10) for $\Lambda = 12500$, with its uniform approximation (solid line). $\beta = 0.9961$.

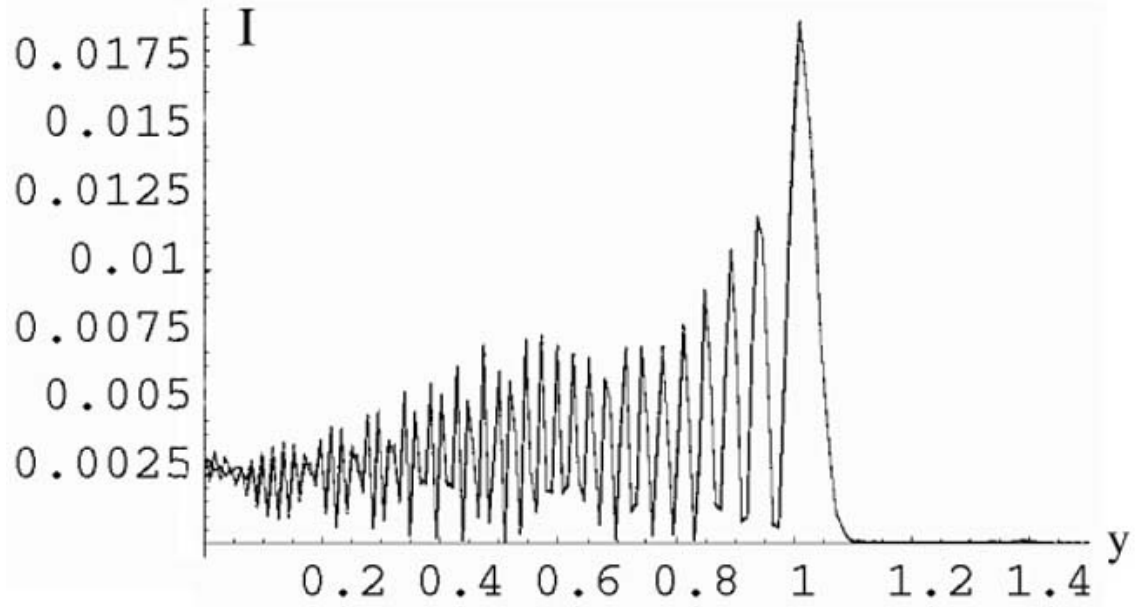


Figure 8: A comparison of the farfield wavefunction obtained by numerical diagonalisation (dashed), with the uniform calculation (solid), for $\Lambda = 12500$ and $\zeta = \pi/2$.

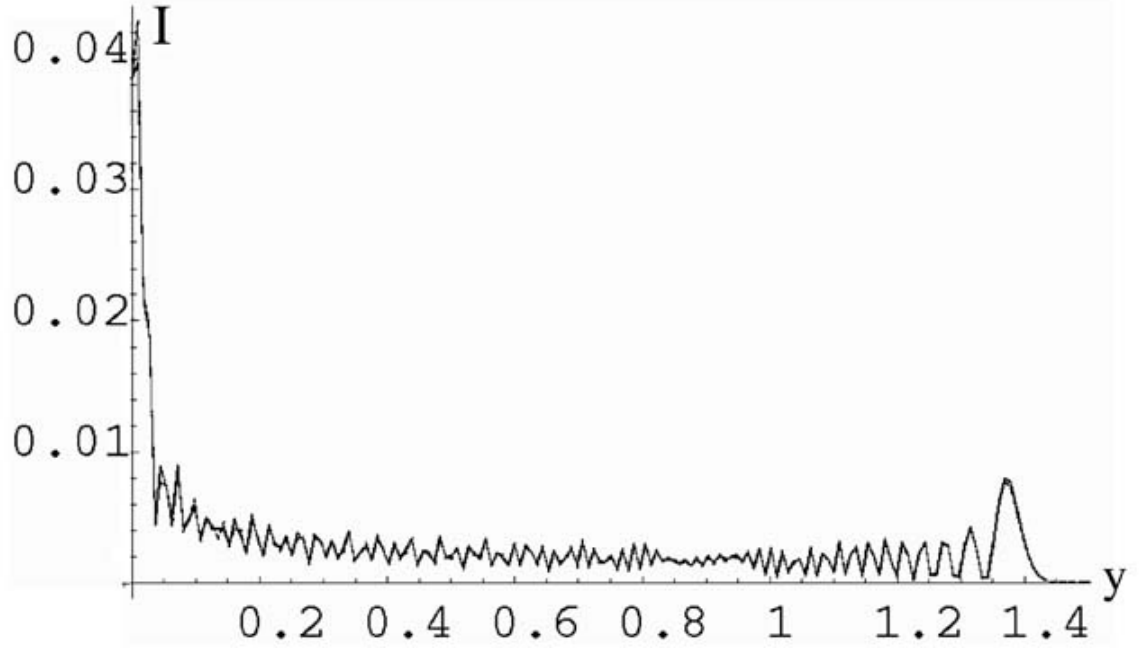


Figure 9: A comparison of the farfield wavefunction obtained by numerical diagonalisation (dashed), with the uniform calculation (solid), for $\Lambda = 12500$ and $\zeta = \pi$.

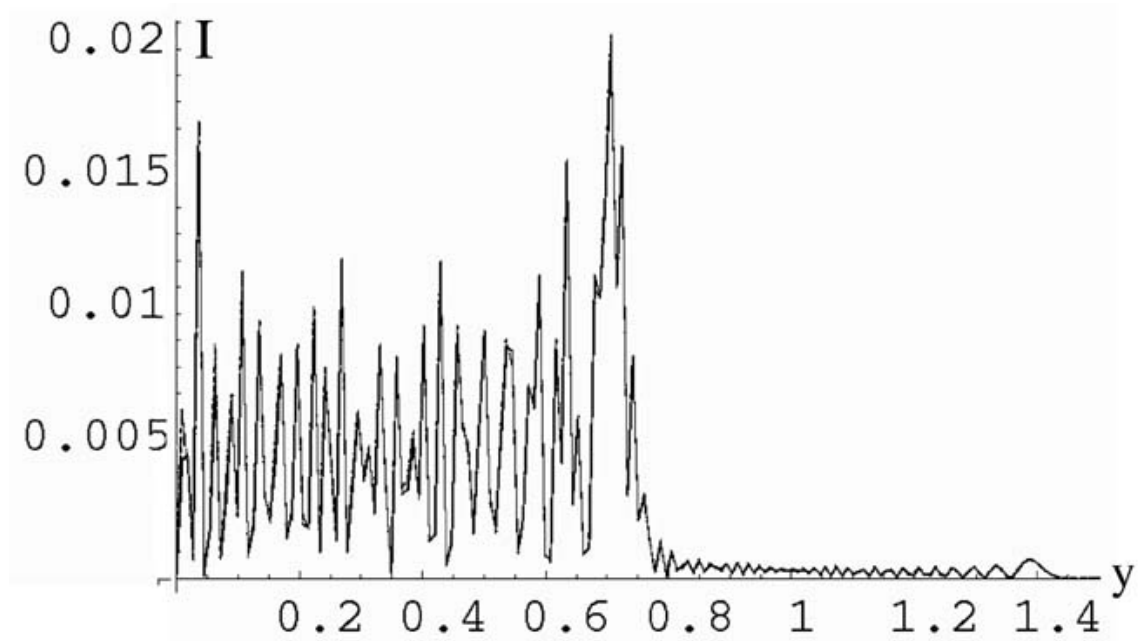


Figure 10: A comparison of the farfield wavefunction obtained by numerical diagonalisation (dashed), with the uniform calculation (solid), for $\Lambda = 12500$ and $\zeta = 3\pi/2$.

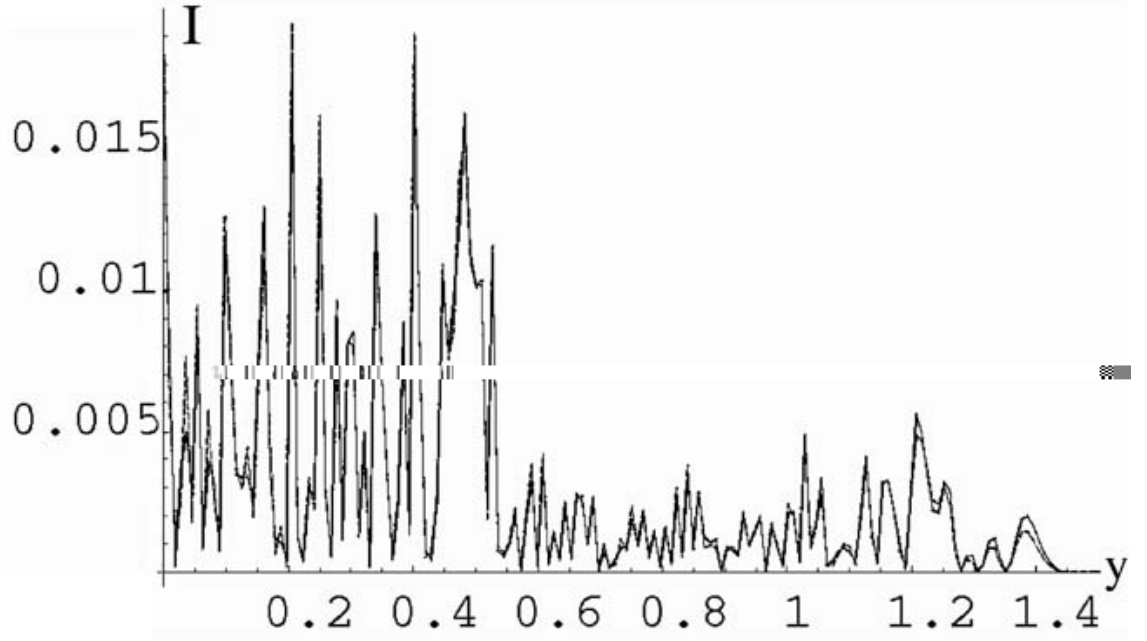


Figure 11: A comparison of the farfield wavefunction obtained by numerical diagonalisation (dashed), with the uniform calculation (solid), for $\Lambda = 12500$ and $\zeta = 7\pi/2$.

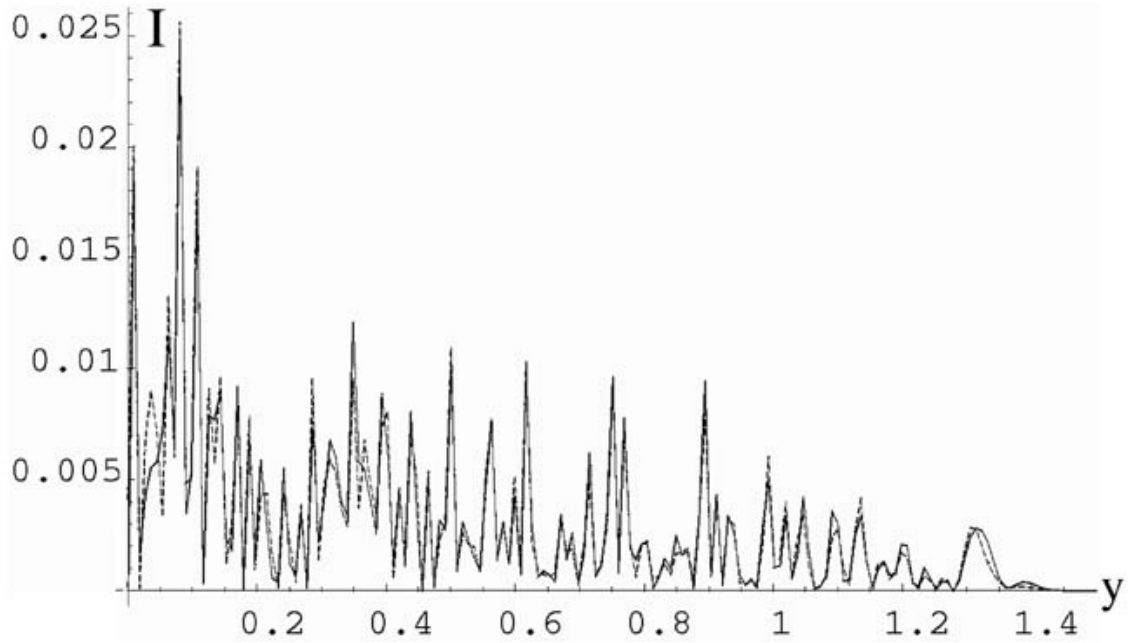


Figure 12: A comparison of the farfield wavefunction obtained by numerical diagonalisation (dashed), with the uniform calculation (solid), for $\Lambda = 12500$: $\zeta = 81\pi/2$.

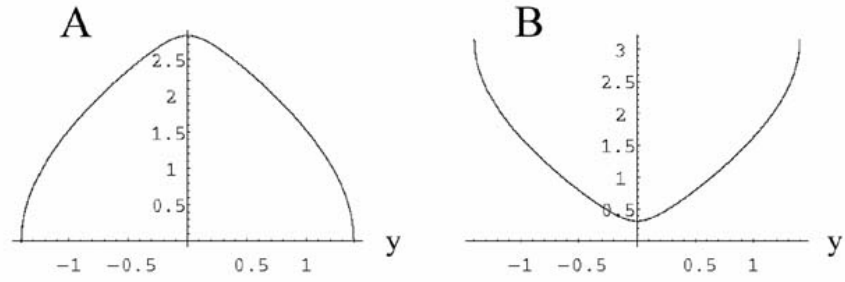


Figure 13: A: The original p_2 , and B: transformed \bar{p}_2 , phase momenta for $\beta = 0.95$.

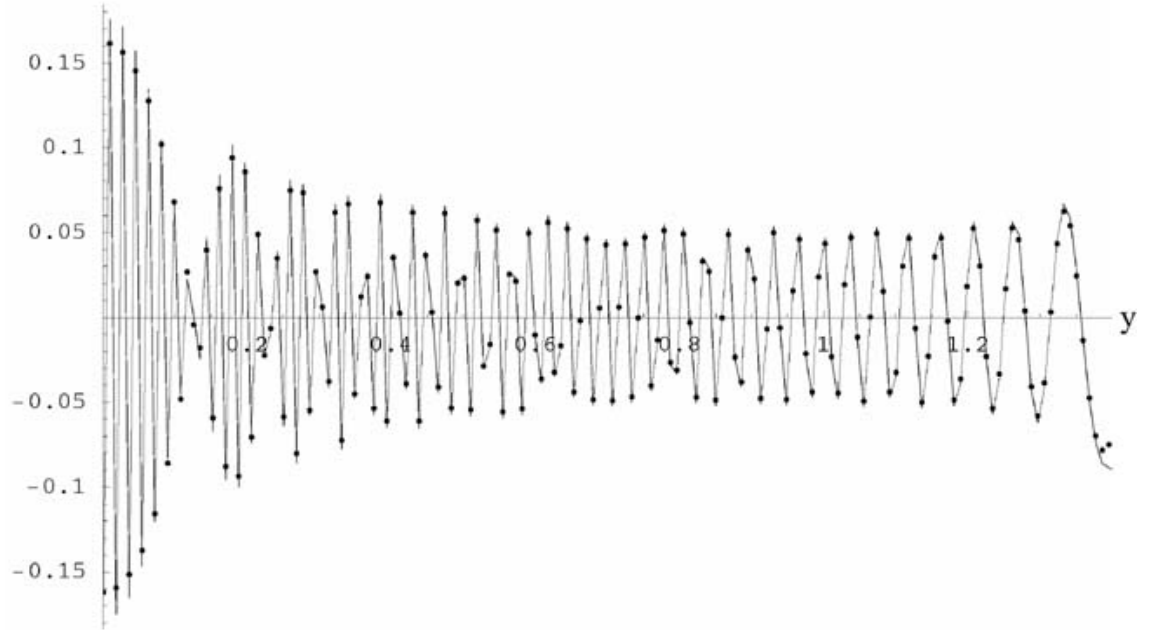


Figure 14: The WKB approximation using the underdense parabolic barrier action, see Equation (71), and the fully numerical solution. In particular, this tests the derived phase angle μ as given by (73). The dots are the numerically calculated points, and the continuous line joins the WKB amplitudes. The value of Λ is 12500 and $\beta = 0.9961$.

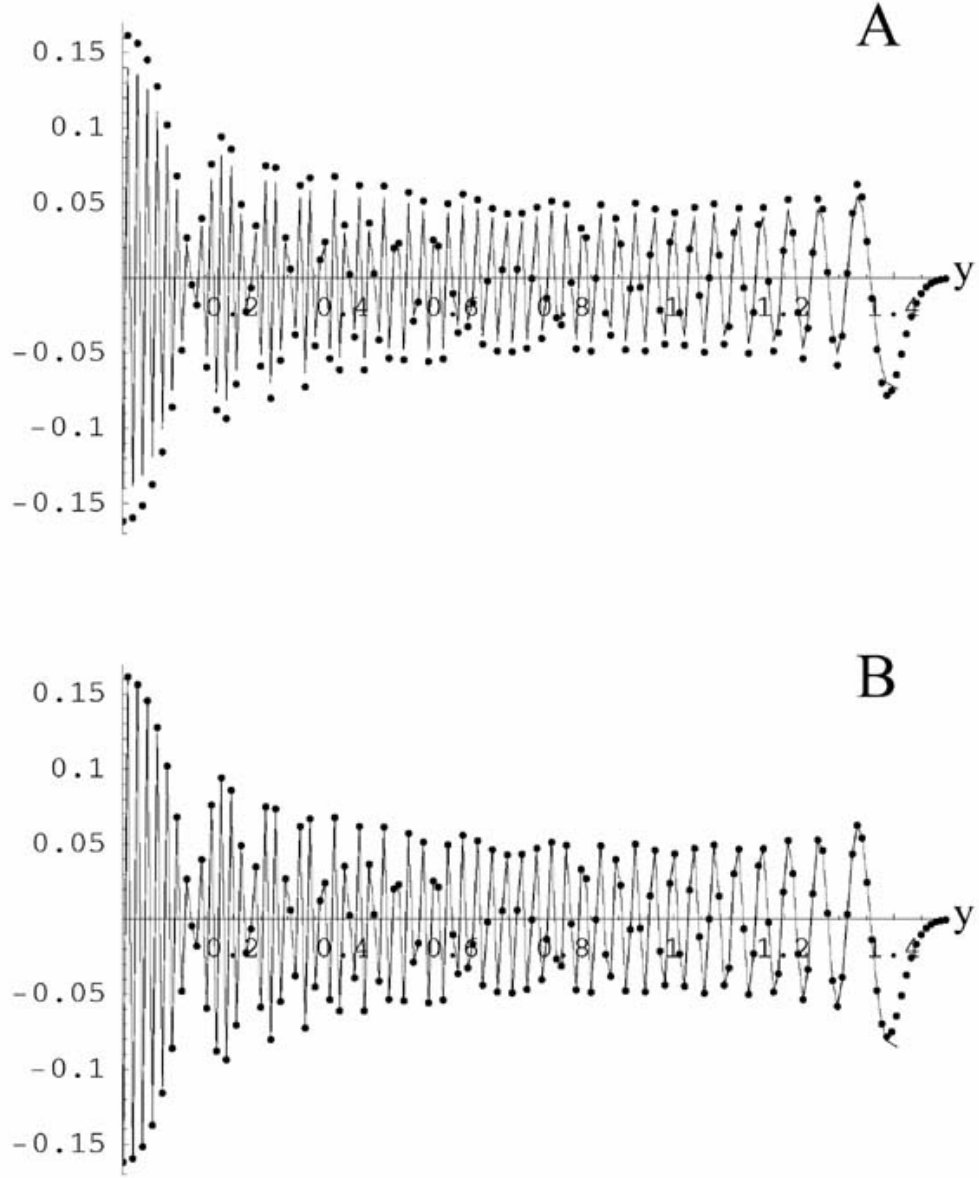


Figure 15: The parabolic barrier transitional approximation: A) as given by Equation (74); B) the renormalised version. The dots are the fully numerical solution. The value of Λ is 12500 and $\beta = 0.9961$.

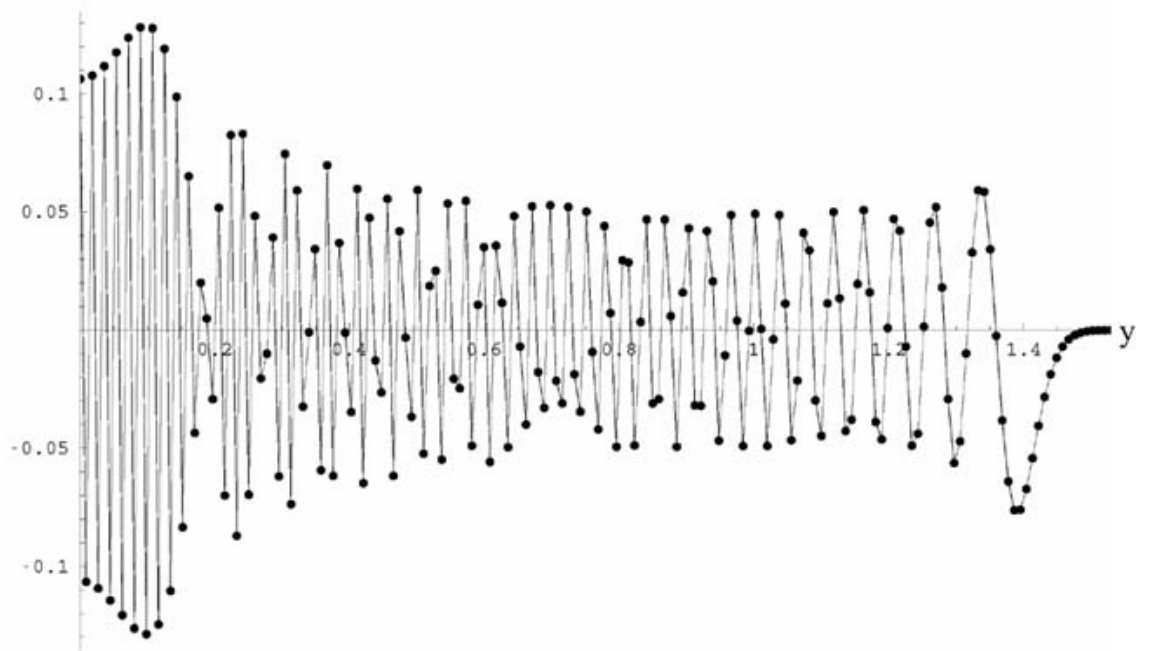


Figure 16: The 201st Bloch wave, which is the first ‘free’ eigenvector. This requires both the overdense parabolic barrier solution, and an Airy function as transitional approximations. The two are joined at the 83rd diffracted beam, which is at $y = 0.742$. The dots are the purely numerical calculation.